Sub-synoptic circulation variability in the Himalayan extreme precipitation event during June 2013

Vellore, Ramesh K.; Bisht, Jagat S.; Krishnan, Raghavan; Uppara, Umakanth; Di Capua, Giorgia; Coumou, Dim

published in
Meteorology and Atmospheric Physics
2020

DOI (link to publisher)
10.1007/s00703-019-00713-5

document version
Publisher's PDF, also known as Version of record

Meteorology and Atmospheric Physics (2020) 132:631–665
https://doi.org/10.1007/s00703-019-00713-5

ORIGINAL PAPER

Sub-synoptic circulation variability in the Himalayan extreme precipitation event during June 2013

Ramesh K. Vellore[1] · Jagat S. Bisht[1,2] · Raghavan Krishnan[1] · Umakanth Uppara[1] · Giorgia Di Capua[3,4] · Dim Coumou[3,4]

Received: 22 May 2019 / Accepted: 11 November 2019 / Published online: 25 November 2019

Abstract

This study investigates the sub-synoptic scale circulation aspects associated with the extreme rainfall event occurred over the North Indian state of Uttarakhand located in the western Himalayas (WH) during the 15–18 June 2013 period. A diagnosis based on hourly ERA5 reanalyzed circulation products archived on finer grids reveals that sustenance of heavy rains during the event period is supported by a propensity of cyclonic vorticity sources channeled toward the WH region through a narrow quasi-steady conduit in the lower troposphere from the ISM circulation. The equatorward segregating mesoscale potential vorticity (PV) structures from the quasi-stationary upper level PV anomaly (trough) during the event administered two pathways for vorticity sources. The first pathway is from the base of the trough culminating into longer horizontal conduit path from the western Arabian Sea, lending perpetual cyclonic vorticity support to the ISM environment. The second pathway is from the right flank of the trough, which promotes sustained environment of deeper mesoscale convergence zone, potentially unstable atmosphere and strong ascent over the Uttarakhand region. The convergence zone is potentially viewed as a region for strong monsoon and extratropical circulation interactions to occur on finer horizontal scales of motion, where significant vertical synchronization of positive PV advection is realized during the 16–17 June 2013 period. In addition to orographic precipitation enhancements, deeper advective synchronization noticed at sub-synoptic time periods is accredited to the nearly doubling 24-h rainfall amounts in the foothill region of Uttarakhand during the event period. The ERA5 diagnosed diabatic heating additionally indicates that precipitating systems at higher (foothill) elevations contribute to upper (lower) tropospheric heat sources.

1 Introduction

The western part of the Himalayas (WH) (Fig. 1) has been constantly witnessing extreme rainfall episodes during the Indian summer monsoon (ISM) months (June–September) in recent decades (e.g., Joshi and Kumar 2006; Rasmussen and Houze 2012; Mujumdar et al. 2012; Nandargi and Gaur 2013; Dobhal et al. 2013; Manish et al. 2013; Chaudhuri et al. 2015; Vellore et al. 2016; Nandargi et al. 2016; Bharti et al. 2016; Priya et al. 2017; Pant et al. 2018). The extreme rainfall categorization follows the convention used by the India Meteorological Department (IMD), i.e., heavy and extremely heavy rainfall days are the days, when 24-h precipitation accumulations are observed to exceed 64.5 mm and 245 mm, respectively (Guhathakurta et al. 2011). Among various intense and torrential rain events reported from the WH region, the extreme rain event occurred over the North Indian state Uttarakhand (see Fig. 1 for the location) during the 15–18 June 2013

Responsible Editor: A.-P. Dimri.

✉ Ramesh K. Vellore
rameshv@tropmet.res.in

[1] Centre for Climate Change Research (CCCR), Indian Institute of Tropical Meteorology (IITM), Pune 411 008, India

[2] Research and Development Centre for Global Change, Japan Agency for Marine Earth Science Technology, Yokohama, Japan

[3] Potsdam Institute for Climate Impact Research, Potsdam, Germany

[4] Institute for Environmental Studies, Vrije Universiteit, Amsterdam, The Netherlands

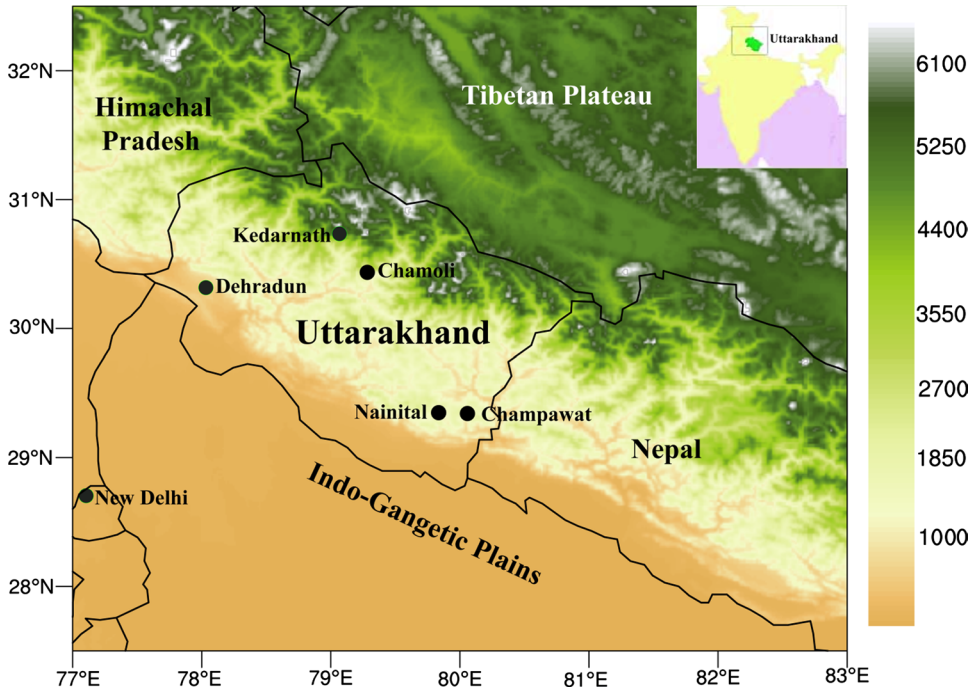

Fig. 1 Topography (shaded; in meters) over the study region. The inset indicates the region of Uttarakhand. Stations (Dehradun, Kedarnath, Chamoli, Nainital, Champawat in Uttarakhand and the Indian capital New Delhi) and the regions referenced in the study are shown on the figure.[Terrain elevations below (above) 2.4 km asl is referred to as the Lesser Himalaya (Greater and Trans Himalaya)] (Source: U.S. Geological Survey)

period has been in the focal point of many recent scientific investigations (see Dobhal et al. 2013; Ray et al. 2014; Kotal et al. 2014; Joseph et al. 2015; Shekhar et al. 2015; Sikka et al. 2015; Vellore et al. 2016; Chevutri and Dimri 2016; Ranalkar et al. 2016a, b; Rajesh et al. 2016; Kumar et al. 2016; Houze et al. 2017; Krishnamurti et al. 2017; Parida et al. 2017; Xavier et al. 2018). These investigations generally concur with the presence of anomalous large-scale extratropical circulation and its interaction with ISM circulation during the period of extreme rains over the WH region. The tenet behind the circulation interactions is a phasing of southward advancing cold/dry extratropical circulation aloft and northward advancing low-level warm/moist ISM circulation. Vellore et al. (2016) additionally indicate that such circulation interactions are more conducive in the background of moderate ISM circulation conditions, i.e., neither active/vigorous nor weak monsoon situations (Rajeevan et al. 2010; Krishnan et al. 2000; Vellore et al. 2014). The circulation interactions tend to favor an environment of increased potential buoyancy in the vicinity of WH foothills and heavy rainfall occurrence follows in concert with orographic lifting of air (e.g., Dubey et al. 2013; Vellore et al. 2016; Hazra et al. 2017; Krishnamurti et al. 2017). Boreal summertime extreme rain episodes are also proposed to have associations with large amplitude quasi-stationary Rossby wave trains within the synoptic wavenumber range between 6 and 8 (Petrukhov et al. 2013; Coumou et al. 2014). Further, a recent study based on complex network methodology indicates that remote influences on extreme rainfall over the Indian region and tropical–extratropical circulation couplings broadly come from upper level Rossby wave-associated physical mechanisms (Boers et al. 2019).

Various observational and numerical modeling studies have examined the unprecedented occurrence of extremely heavy precipitation over the Uttarakhand region during the period 15–18 June 2013 (e.g., Houze et al. 2017; Krishnamurti et al. 2017; see the references therein). Nonetheless, the sub-synoptic scale complement to the dynamics of large-scale circulation interactions during the event period largely lacks pellucidity from these investigations—in particular, from the viewpoint of longer span of torrential rains and significant spatiotemporal variability in rainfall intensities observed over the mountainous terrain of Uttarakhand during the event period (cf. Table 1 and Fig. 1 of Ranalkar et al. 2016a). Vellore et al. (2016) briefly highlighted the finer scale circulation responses across the WH region during the event period based on the unbalanced mesoscale circulation aloft and mesoscale orographic forcing. Some studies also point out that long-lived convective systems can be promoted by favorable wind shear environment along the windward side of the mountains, as well as through convective regenerative mechanisms (e.g., Maddox et al. 1979; Doswell 1987; Romero et al. 2000; Foresti and Pozdnoukhov 2012; Soderholm et al. 2014). In this context, Kotal et al. (2014) surmised on the circumstances of regenerative mesoscale convective cell generations to longer span of torrential rains during the event period. They also suggested the possibility of a low-level convergence zone development as a consequence from circulation interactions. Rajesh et al.

(2016) also recognized from the coarser reanalysis products that there is a harmonization of upper level potential vorticity (PV) and low-level moisture convergence to favor the precipitation enhancements over the WH region during the event period. However, their study clearly pinpointed the criticality of requirement of much finer spatiotemporal analyses for better insights into the prognosis of mesoscale PV processes and interaction mechanisms.

In view of the large equivocation from the aforesaid studies, the finer scale augmentations to large-scale circulation environment during the extreme precipitation period clearly recall for better comprehensibility. More particularly on rationales of regional scale convergence zones and other possible dynamical mechanisms are in support of circulation maintenance and longevity of the Himalayan precipitation during the event period. In this study, we intend to provide some insights into this issue by primarily focusing on the finer scale spatiotemporal sub-synoptic details during the event period. The latest European reanalysis ERA5 datasets (Hersbach and Dee 2016; https://cds.climate.copernicus.eu) archived at hourly intervals on finer horizontal grids ($0.3° \times 0.3°$ grid resolution) are used for the analysis. Observational analyses also include the infrared (IR) radiance/imagery data archived at 30 min intervals from the Meteosat-7 geostationary meteorological satellite (https://eoportal.eumetsat.int) and the Tropical Rainfall Measuring Mission (TRMM; Huffman et al. 2007; https://pmm.nasa.gov) precipitation products. The observations and circulation diagnostics for this event from ERA5 are given in the following.

2 Observations and ERA5 circulation diagnostics

To begin with a succinct retrospect of large-scale circulation aspects from earlier studies focused on this event, the ISM circulation rapidly progressed northward toward the region of Uttarakhand Himalayas (see Fig. 1 for the location) during the event period in mid-June 2013 much earlier than the normal precipitation onset for this region. The large-scale environment at upper levels during this time includes: (1) rapid ridge intensification and blocked anticyclonic circulation over the western part of Eurasia, (2) baroclinically amplifying upper level trough from Russia concurrent with Rossby wave-breaking (see also Sect. 3.1) signatures in the middle latitudes, and (3) significant splitting of the Tibetan anticyclone (Hsu and Plumb 2000; Popovic and Plumb 2001; Vellore et al. 2016) in the subtropical latitudes. In consequence to this evolution, the downstream environment of the aforesaid intensifying ridge resulted in upper level westerly trough thinned and intruded far equatorward into the tropical latitudes, and also exerted strong upper level jet accelerations poleward of the WH region.

2.1 Rainfall

The reader is referred to the following literatures Kotal et al. (2014), Ray et al. (2014), Sikka et al. (2015), Ranalkar et al. (2016a; b), where rain gauge observations during the event period are reported in detail and is briefly presented here. Confined regions of observed heavy downpour during the period 15–18 June 2013 over the Indian state of Uttarakhand state and neighborhood were attributed to multi-day incessant rains. The highest percentage of rainfall departure (+ 191%) from the climatological normal is seen over this region in June 2013 and this profound excess came from this particular event (e.g., Sikka et al. 2015; Kaur and Purohit 2014). Figure 2a shows the spatial distribution of 24-h precipitation accumulations from TRMM. One can see that precipitation accumulations were rather widespread extending from the northwest Indian states to western part of Uttarakhand on 15 June 2013. The extreme rainfall conditions began to confine over the western and eastern parts of Uttarakhand during the subsequent 2 days (see also Fig. 2 of Kotal et al. 2014; Shekhar et al. 2015). The 24-h observed precipitation totals ending at 16, 17, and 18 June 2013 from 24 foothill stations of Uttarakhand state were 2170, 3716, 1978 mm, respectively, and the reported mean subdivisional rainfall from various districts of Uttarakhand was 72, 134, and 81 mm, respectively (Ray et al. 2014; cf. Table 1 of Ranalkar et al. 2016a). One can clearly notice that nearly twice large amounts of 24-h rainfall accumulations were reported from lower foothill elevations on 17 June 2013, i.e., during the period 03 UTC 16 June 2013–03 UTC 17 June 2013. Table 1 shows observed 24-h precipitation accumulations during this period from various stations located over the Lesser Himalayan elevations (< 2.4 km asl) of North Indian states Uttarakhand and Himachal Pradesh (see Fig. 1 for the regions). Note that the two neighboring lower foothill stations Dehradun and Kalsi (see Table 1 for the elevations and locations) in Uttarakhand received extremely heavy 24-h rainfall accumulations of 338 mm and 370 mm, respectively. This is also + 375% above the daily normal values for this day (Srivatava and Guhathakartha 2013; Dube et al. 2014). Also another station, Paonta in proximity to these two stations located on the northeastern part of Himachal Pradesh also received 24-h accumulations of 410 mm (see also Fig. 3 of Kotal et al. 2014; Ray et al. 2014). More stations located over the eastern part of Uttarakhand such as Haldwani (see Table 1 for the location and elevation), Nainital, and Champawat (see Fig. 1 for the locations) reported extreme rains (exceeding 200 mm) during the 24-h period ending on 18 June 2013 (Ray et al. 2014). Interestingly, data sparse higher elevation locations of Uttarakhand (e.g., Kedarnath; see Fig. 1 for the location) reported relatively lesser 24-h rain accumulations as compared to the lower elevations. For example, the reported mean rainfall from an observatory

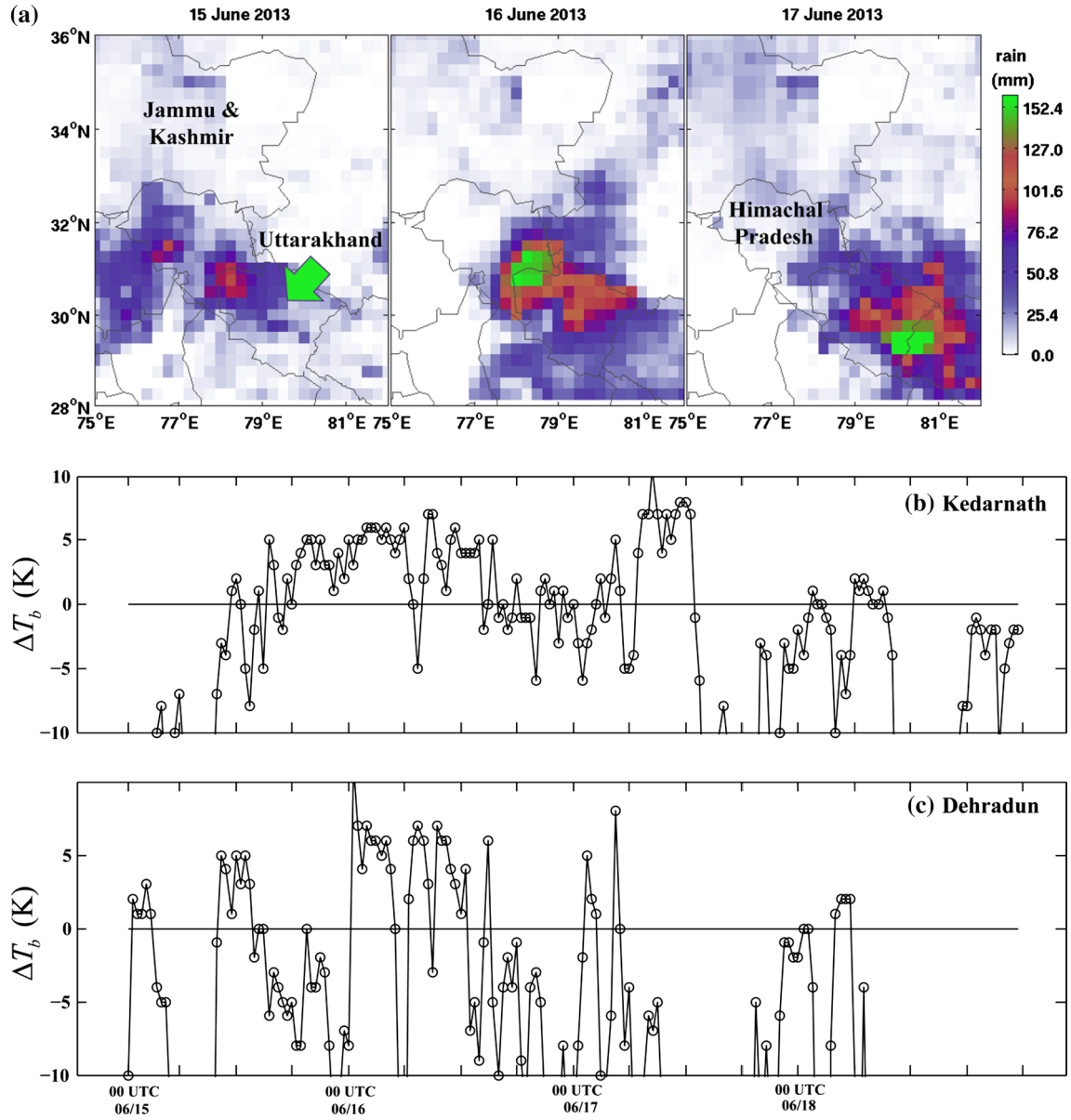

Fig. 2 **a** 24-h precipitation accumulations (mm) over the northern part of India from TRMM. **b**, **c** Hourly brightness temperature differences diagnosed from METEOSAT-7 infrared satellite products during 15–19 June 2013 over **b** Kedarnath and **c** Dehradun

near Kedarnath was 107 mm day^{-1} and 70 mm day^{-1} at Chamoli (see Fig. 1 for the location) during the 15–17 June 2013 period [Dobhal et al. 2013 (cf. Fig. 2); Ray et al. 2014 (cf. Table 3.4)].

2.2 Circulation

Figure 3 shows the ERA5 reanalyzed 700 hPa and 500 hPa horizontal winds, geopotential heights, and horizontal wind convergence for the period 14–17 June 2013. The synoptic setup on 14 June 2013 includes two distinct meso-α scale (200–2000 km; Orlanksi 1975) cyclonic circulation environment, where the first is associated with the monsoon low (ML) centered at 20° N, 84° E originated from northwest Bay of Bengal prior to this time. The second is an offshore cyclonic circulation in the lower troposphere centered at 20° N, 66° E over northern Arabian Sea (Fig. 3a–d). The former shows a west–northwest movement in time, while the latter remains nearly quasi-steady which becomes less apparent and merges with the former after 15 June 2013. Closed isolines of geopotential heights over the central part of India show a tendency of tilting in southwest–northeast direction. The moisture-laden air streams along the southern and eastern flanks of the circulation around the ML are directed

Table 1 Observed 24-h precipitation accumulations (mm) ending at 0300 UTC 17 June 2013 over the Uttarakhand region (see also Kotal et al. 2014; Ranalkar et al. 2016a, b)

Station name	Latitude (°N), longitude (°E)	Elevation (m)	Rainfall (mm)
Dehradun	30.32, 78.05	667	370
Purola	30.87, 78.08	1503	410
Haridwar	29.92, 78.12	276	220
Uttarkashi	30.73, 78.43	1297	210
Tehri	30.37, 78.43	1672	170
Mussorie	30.46, 78.07	1836	150
Devprayag	30.14, 78.60	785	160
Roorkee	29.84, 77.92	254	150
Kirtinagar	30.21, 78.75	748	100
Rudraprayag	30.28, 78.98	973	90
Karnaprayag	30.26, 79.22	981	90
Jollygrant	30.19, 78.18	553	224
Ranichauri	30.20, 78.52	1592	205
Rishikesh	30.11, 78.28	371	145
Kalsi	30.53, 77.84	558	391
Srinagar	30.22, 78.77	688	133
Mukteshwar	29.46, 79.66	2047	240
Kausani	29.84, 79.60	1673	210
Haldwani	29.22, 79.51	421	200
Nainital	29.36,79.46	1747	180
Champawat	29.34, 80.09	1650	100
Pithoragarh	29.57, 80.23	1523	69
Almora	29.59, 79.65	1432	90
Matela	29.62, 79.62	1211	97
Pantnagar	29.02, 79.48	232	58
Ramnagar	29.39, 79.11	354	56
Ranikhet	29.64, 79.42	1700	43
Pati	29.40, 79.93	1520	206
Lohaghat	29.40, 80.09	1670	139
Sitarganj	28.93, 79.70	198	75
Gangolihat	29.65, 80.04	1718	103
Bageshwar	29.83, 79.77	1020	160
Joshimath	30.55, 79.57	2146	110
Jakholi	30.39, 78.89	1539	110
Chamoli	30.29, 79.56	2199	80
Tharali	30.07, 79.50	1458	170
Bharsar	30.05, 79.00	2247	122
Dhanauri	29.93, 77.97	269	151
Mean			157.5

toward the WH region during the event period (Fig. 3e–h). A strong meridional momentum on the eastern flank of the ML is noted, which is facilitated by the sharp zonal height gradients and a quadruple pattern of low (meridional orientation) and high (zonal orientation) pressure environments evident at mid-levels centered over northern part of India.

Two distinct small amplitude or shortwave ridge patterns (red-dashed lines in Fig. 3) at mid-levels are noticed on mesoscale below the zonally shed parts of the large-scale Tibetan anticyclone at upper levels (see Vellore et al. 2016; see also Fig. 7a, b). Notice that the shortwave ridge pattern from the eastern shed part is strongly influenced by flow interactions with the high terrain of the Himalayas and distinctly protrudes into the front flank of upper level trough (Fig. 3g). One can normally expect that small amplitude ridges generally tend to weaken as they move into large amplitude wave troughs at upper levels. However, there is a prevalence of this shortwave ridge pattern during the entire event period due to slow eastward progression and rapid southward progression of the upper level westerly trough (Fig. 3k). Also, a synoptic scale ascent is however limited with the movement of this shortwave ridge pattern over the Himalayan terrain, but warm air advection supported by ridging coupled with orographic ascent could promote the precipitation. The other ridge pattern is relatively weaker, which extends from the Arabian Peninsula toward northwestern part of India (Fig. 3e, g). Note that meridional evolution of anticyclone located to the west of the ML is, rather rapid compared to its zonal expansion, i.e., the eastward extension of ridge over the Arabian Peninsula is constricted by the far equatorward extent of the upper level trough (see the 5800 m isoline in Fig. 3i, k). Significant mesoscale wind convergence regions (or fringes of cyclonic vorticity) resulting from zonal wind shear are evident from lower-to-mid levels, notable are the one moving toward Uttarakhand region from northwest and other from the Arabian Sea (Fig. 3i–l). The northward movement of ML is apparently promoted more by the anticyclonic tendency in relative vorticity (e.g., Anthes and Hoke 1975) on the eastern side of the ML and less westward drift by β-effect. The sharp zonal gradients in height (v-wind) field tend to enhance the lower-to-mid level cyclonic vorticity on the eastern flank of the ML. The high-pressure environment to its east aids to align the plumes of cyclonic vorticity directed toward the WH region in an organized manner from the Arabian Sea. Also, it aligns the upper level flow normal toward the WH region, thereby providing a veering wind structure in the vicinity of Uttarakhand region (e.g., Fig. 3g, h). Thus, the Uttarakhand region during the event period is thermally separated by warm air advection (also an area of isentropic lifting) from its east and equatorward advancing cold air from its west together with perpetual supply of cyclonic vorticity sources from the ISM environment.

The vertical structure of horizontal winds in the vicinity of the WH region shows east–southeasterly (along-barrier winds) at low levels, while southerlies (normal to the WH barrier) are seen at upper levels from the downstream environment of the equatorward deepening westerly trough at and later than 15 June 2013. Such sheared wind structure in the vertical on the windward side of the mountains

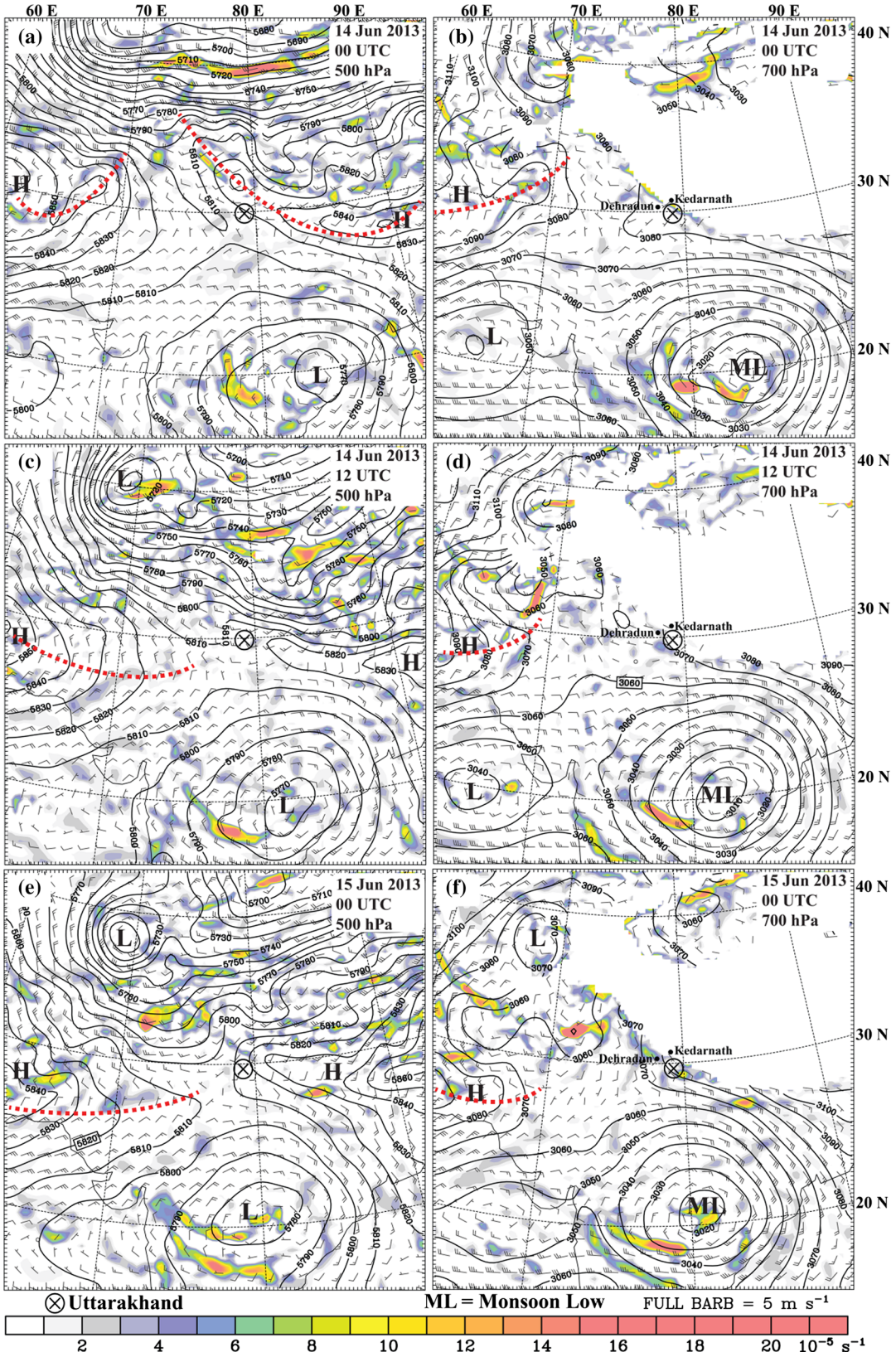

Fig. 3 500 hPa (left panel) and 700 (right panel) hPa geopotential heights (m), horizontal winds (full barb = 5 m s^{-1}) and horizontal wind convergence (shaded; $\times 10^{-5}$ s^{-1}) during the period 14–17 June 2013. Locations of Dehradun and Kedarnath are indicated on the figure. L and H are low-pressure and high-pressure markers. *ML* Monsoon low (Source: ERA5 reanalysis)

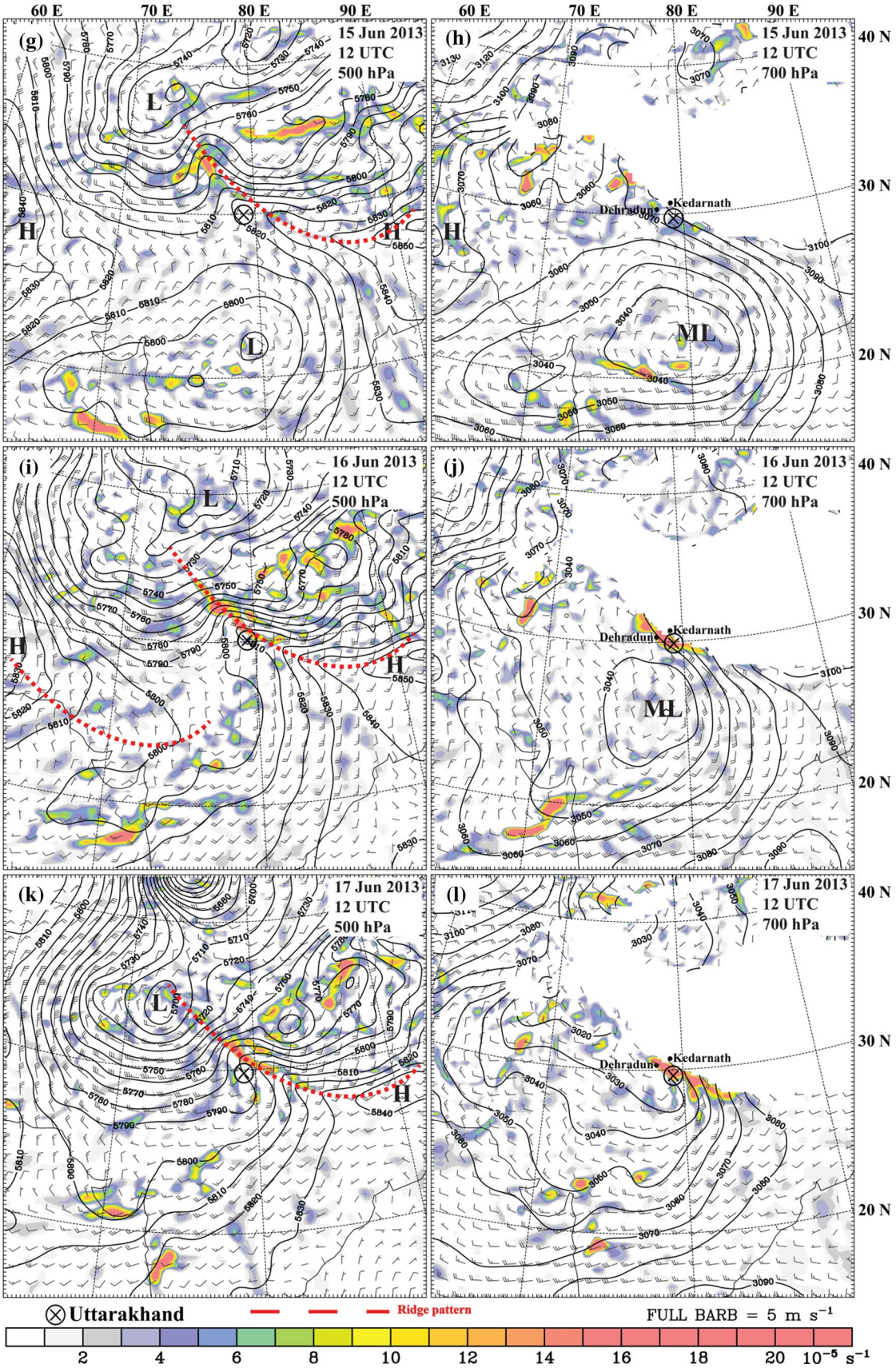

Fig. 3 (continued)

is also conceptualized to favor quasi-stationary terrain-locked convection and repeated development of convective cells at the same location along idealized mountain ridges (Soderholm et al. 2014). Some studies further indicate that windward side mountain slopes are preferred regions for precipitation enhancements from meso-γ scale stationary rainfall cells (Foresti and Pozdnoukhov 2012). As also will be seen later, a narrow region of high PV air, where the vorticity acquired from the cyclonic tendency of air parcels traversing southward to regions of lower Coriolis parameter *f* is funneled over the Arabian Sea (~ along 20° N) and penetrate into the ISM environment (see also Fig. 8d). Briefly, the ISM environment exhibits a cyclonically curved (warm) conduit trajectory through which air streams possessing cyclonic vorticity are channeled toward the western Himalayan foothills. The quasi-steady mid-level ridging patterns from both sides of the ISM environment and dry air advection from extratropics into the northwestern parts of India constantly tend to confine this conduit trajectory intact during the event period.

2.3 Satellite imagery

The aforementioned conduit trajectory can be clearly noticed from the METEOSAT-7 infrared satellite cloud imagery shown in Fig. 4a, where the conduit heads to west of the Uttarakhand region on 15 and 16 June 2013, while it tilts to east of this region from 17 June 2013 as the lower tropospheric height low moves closer to this region (see Fig. 3j, l). It is also noted from multi-spectral satellite observations (METEOSAT and TRMM) that distinct regions of significantly colder cloud tops (brightness temperatures less than 210 K) embedded within the mesoscale organization of clouds are seen over the Uttarakhand region during the periods of intense rain activity (see also Houze et al. 2017). These colder cloud tops are often regions of cloud systems with possible overshooting tops where unstable tropospheric

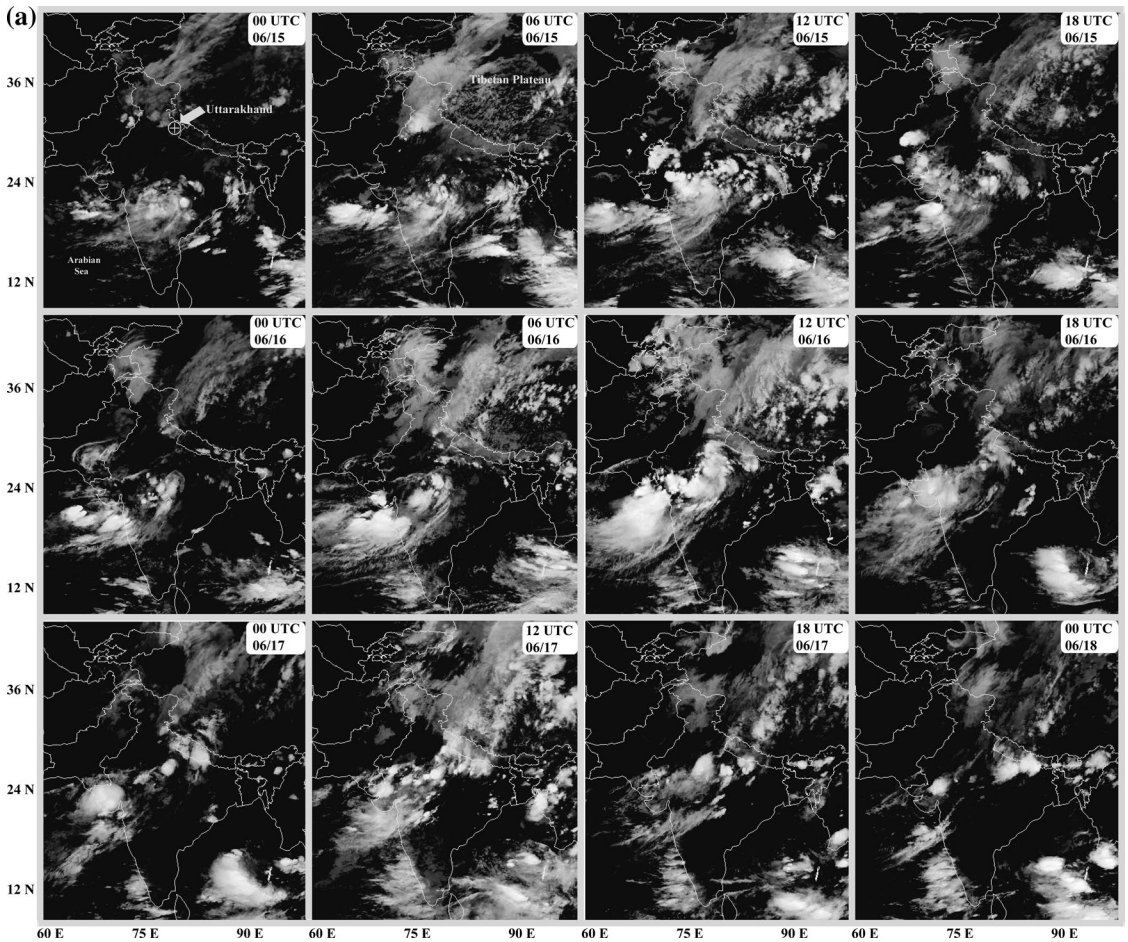

Fig. 4 **a** Six-hourly METEOSAT-7 infrared satellite imagery shown for the period 15–18 June 2013. Location of Uttarakhand (see also Fig. 1) is marked by ⊕ indicated by an arrow on the top figure (Source: https://eoportal.eumetsat.int). **b** Hourly METEOSAT-7 infrared satellite imagery during 15–16 June 2013 over the Uttarakhand region. Shaded are the brightness temperatures (units in K). Dehradun district, Uttarakhand is marked by ⊗ (Source: https://eoportal.eumetsat.int)

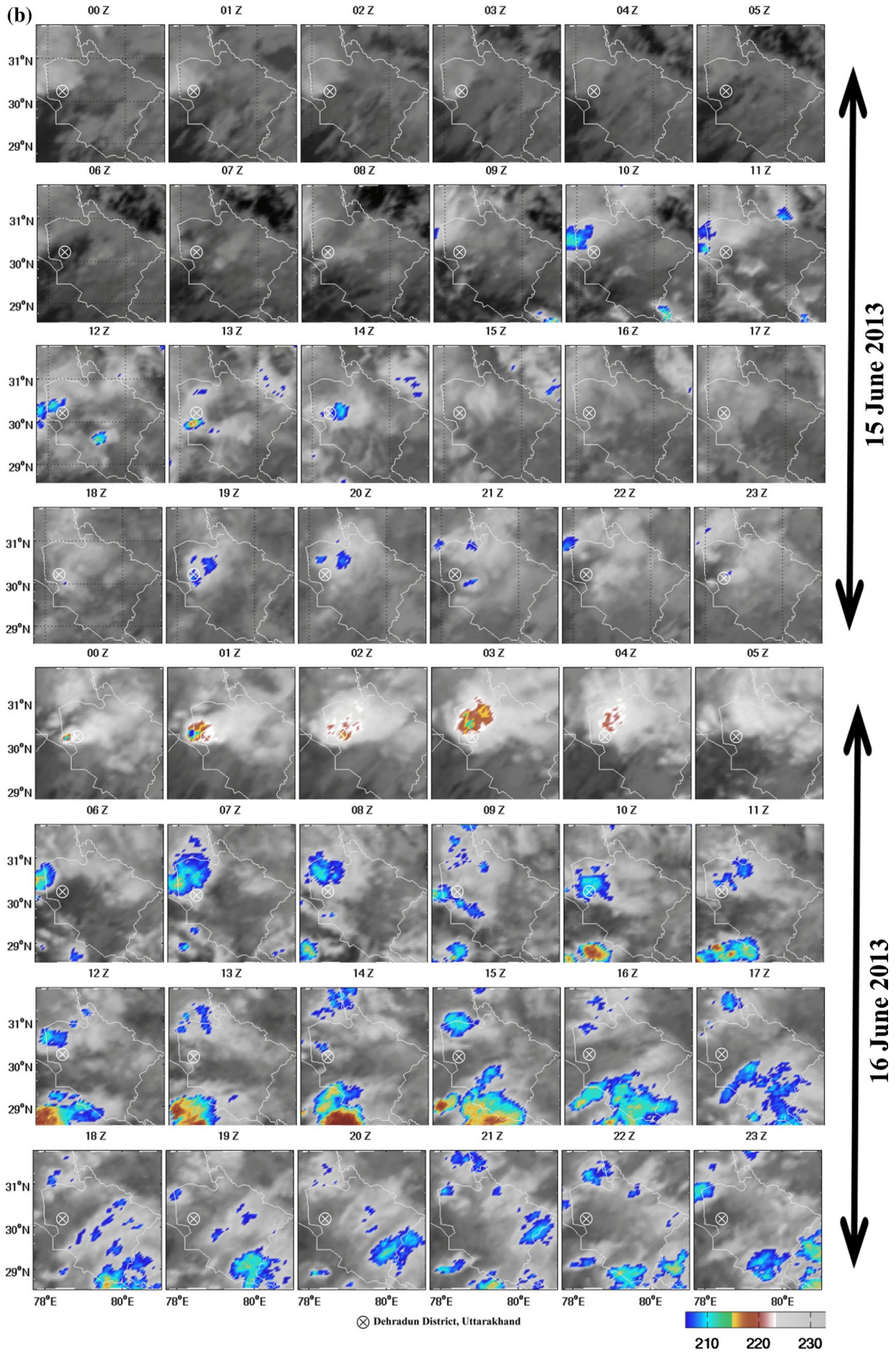

Fig. 4 (continued)

air can penetrate into stable regions of stratosphere (e.g., Schmetz et al.1997; Bedka et al. 2010). Krishnamurti et al. (2017) also indicated convective clouds of greater vertical extent across the WH region during this event from the limitedly available satellite passes of the CALIPSO (https://eowweb.larc.nasa.gov/PRODOCS/calipso). The Kalpana-1 infrared satellite imagery also indicated organized cloud pattern seen to the poleward regions of Uttarakhand during the event period with cloud top temperatures (CTTs) ranging between − 40 and − 20 °C (see Kotal et al. 2014), while CTTs as low as − 80 °C in association with deep convection were generally prevalent over the northern Arabian Sea (not shown).

Hourly infrared satellite imagery from METEOSAT-7 focused over the Uttarakhand region on 15 and 16 June 2013 is shown in Fig. 4b. One can clearly see pockets of colder cloud tops from 10 UTC 15 June 2013 in the vicinity of Dehradun over the western side of Uttarakhand State, while more organized cloud clusters on meso-β scale (20–200 km) is noticeable from 16 June 2013 both over the western and southeastern parts of Uttarakhand. Notice that the western districts Dehradun and Uttarkashi exhibit colder mesoscale cloud tops embedded within the organized cloud pattern spread over the western part of Uttarakhand during the 06–15 UTC 16 June 2013 period, when extreme hourly rains were reported from these locations. Figure 2b, c shows the time series of brightness temperature (BT) differences (between IR band: 10.5–12.5 μm and water vapor absorption band: 5.7–7.1 μm), where larger positive BT differences are interpreted as convective cells of larger vertical extent (Schmetz et al. 1997). Note that positive BT differences are seen in a continuous manner at Kedarnath (higher elevation; see Fig. 1) during the 15–16 June 2013 period, while Dehradun (foothill station) shows such positive BT differences only at intermittent spans on 16 June 2013. That is, cloud columns with colder cloud tops are largely noticed over the foothill region, while the temporal evolution of CTTs indicates slightly warmer cloud tops at higher elevations indicating the presence of shallower, but more organized stratiform-type precipitating systems (see also Houze et al. 2017).

2.4 Thermodynamic background and diabatic heating

Thermodynamic analysis from ERA5 indicates that the western part of Uttarakhand in the vicinity of Dehradun (see Fig. 1 for the location) exhibits strong convective instability during the period 13–16 June 2013. Briefly, a thermodynamic environment of potentially unstable air (local change of equivalent potential temperature θ_e with height is negative; North and Erukhimova 2009; see also the review by Krishbaum et al. 2018) with greater probabilities of severe convection is recognized in the vicinity of Uttarakhand region. Figure 5a–e show a planview of water vapor mixing ratios and pressure diagnosed on $\theta = 325$ K surface during the period 15–18 June 2013. Figure 5g–l show the humidity parameters along the vertical cross-section A''–B (shown in Fig. 5d) during the same period. One can clearly notice stronger transport of moisture by the monsoon winds along the conduit and isentropic ascent (winds crossing isobars) in the vicinity of WH region. This is markedly separated by dry descending air located to its west whose equatorward extension is far into tropical latitudes. There is a sharp zonal moisture contrast across northwestern part of India and a distinct tongue of lower mixing ratios are seen over the region immediate south of Uttarakhand in association with southward advancing dry air intrusions (Fig. 5a–f). A near saturation (lower relative humidity) seen within 800–400 hPa (below 800 hPa) over the Indo-Gangetic Plains and along the foothill region on 15 June 2013 substantiates potentially unstable environment in the vicinity of Uttarakhand region (Fig. 5g). Also notice the deeper transition zone located to the west of Uttarakhand region distinctly separates the subtropical dry air descent and humid monsoon air. There is a perpetual downward advancement of dry air from mid-to-lower levels and a narrow region of sharp relative humidity contrast (similar to a moisture front) seen to the west of Dehradun and Kedarnath in Uttarakhand (Fig. 5g–l). In an airmass sense, this mesoscale moisture front in the vertical bears some resemblance with the dry line or dry front seen horizontally over the U.S. Southern Plains (e.g., Fujita 1958; Hoch and Markowski 2005). One can clearly envisage a convective triggering from lifting of moist air over the Uttarakhand region ahead of the subtropical dry air descent. This dry air descent also serves as a shield by not letting the monsoon air penetrating further west of Uttarakhand in time.

Therefore, looking at the contrasting rainfall intensities between lower and high elevations of Uttarakhand (Kotal et al. 2014; Ranalkar et al. 2016a, b) during the event period, one can presume that larger sub-synoptic rain amounts appear to have come from shorter, but copious rain spells from less-organized convection with possibilities of convective cell regeneration or stationary convective cells at the same location over the western districts of Uttarakhand. At the same time, relatively less abundant hourly rain amounts, but more incessant for longer periods came from more organized cloud clusters at higher elevations. The column-integrated mean (850–200 hPa) diabatic heating, following Yanai et al. (1973), diagnosed from ERA5 is shown in Fig. 6 to further exemplify this conjecture. One can clearly see profound latent heat release over the Uttarakhand region from extreme rain activity during the 15–17 June 2013 period and also a moist convective environment along the conduit trajectory. There are clear indications of a trail of cyclonic vorticity sources from the northern Arabian Sea marching toward the WH foothills

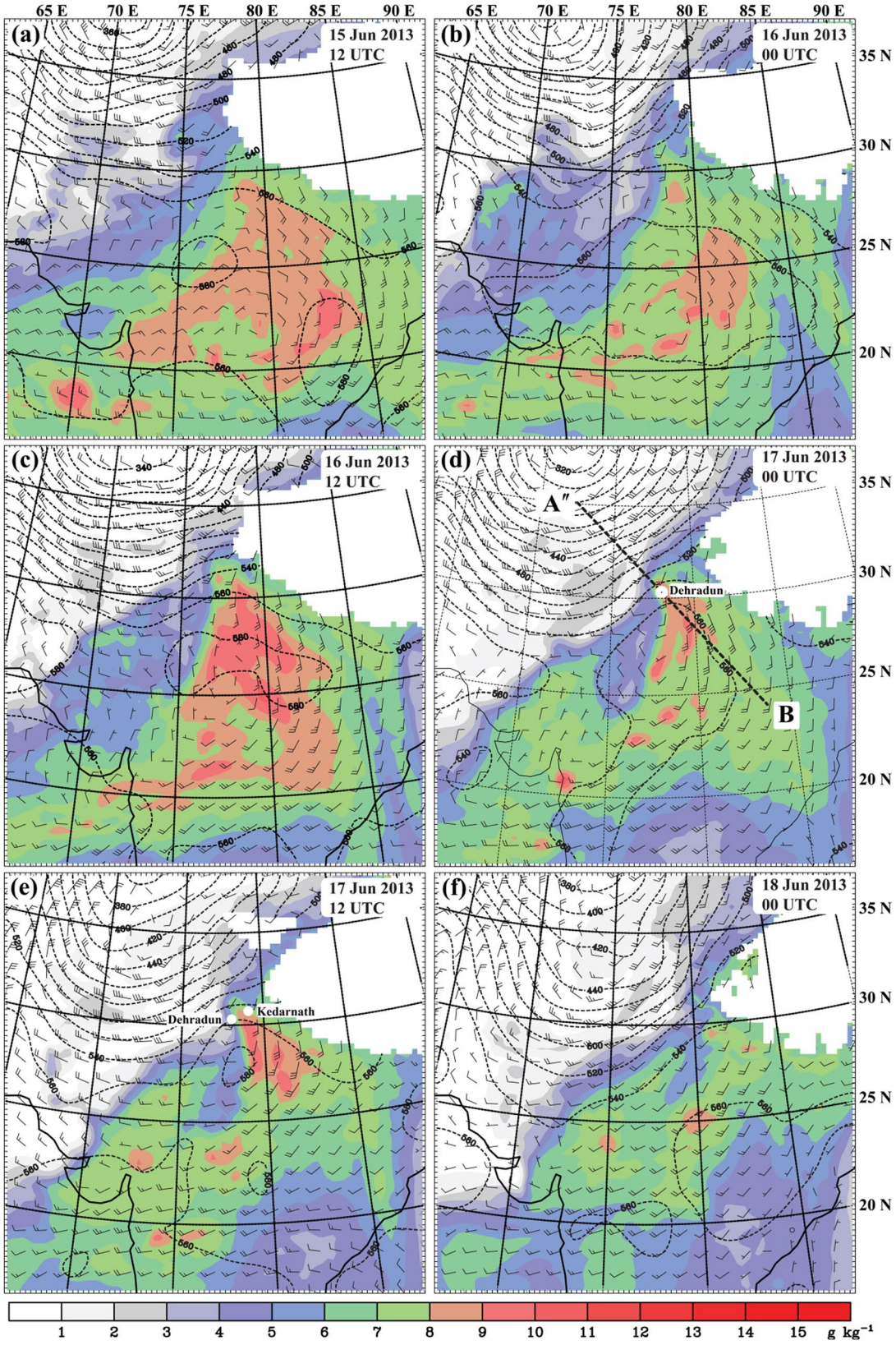

Fig. 5 **a**–**f** Planview of water vapor mixing ratio (shaded; g kg^{-1}), isobars (dashed line; hPa), and horizontal winds (full barb = 5 m s^{-1}) on θ = 325 K surface during the period 15–18 June 2013. **g**–**l** Vertical view of water vapor mixing ratio (solid contours; g kg^{-1}), relative humidity (shaded; %) and dew point depressions (dashed contours; in °C) along the cross-section *A*″–B shown in **d**. Locations of Dehradun and Kedarnath in Uttarakhand are shown on the figure. Dark arrows indicate dry air intrusions (Source: ERA5 reanalysis)

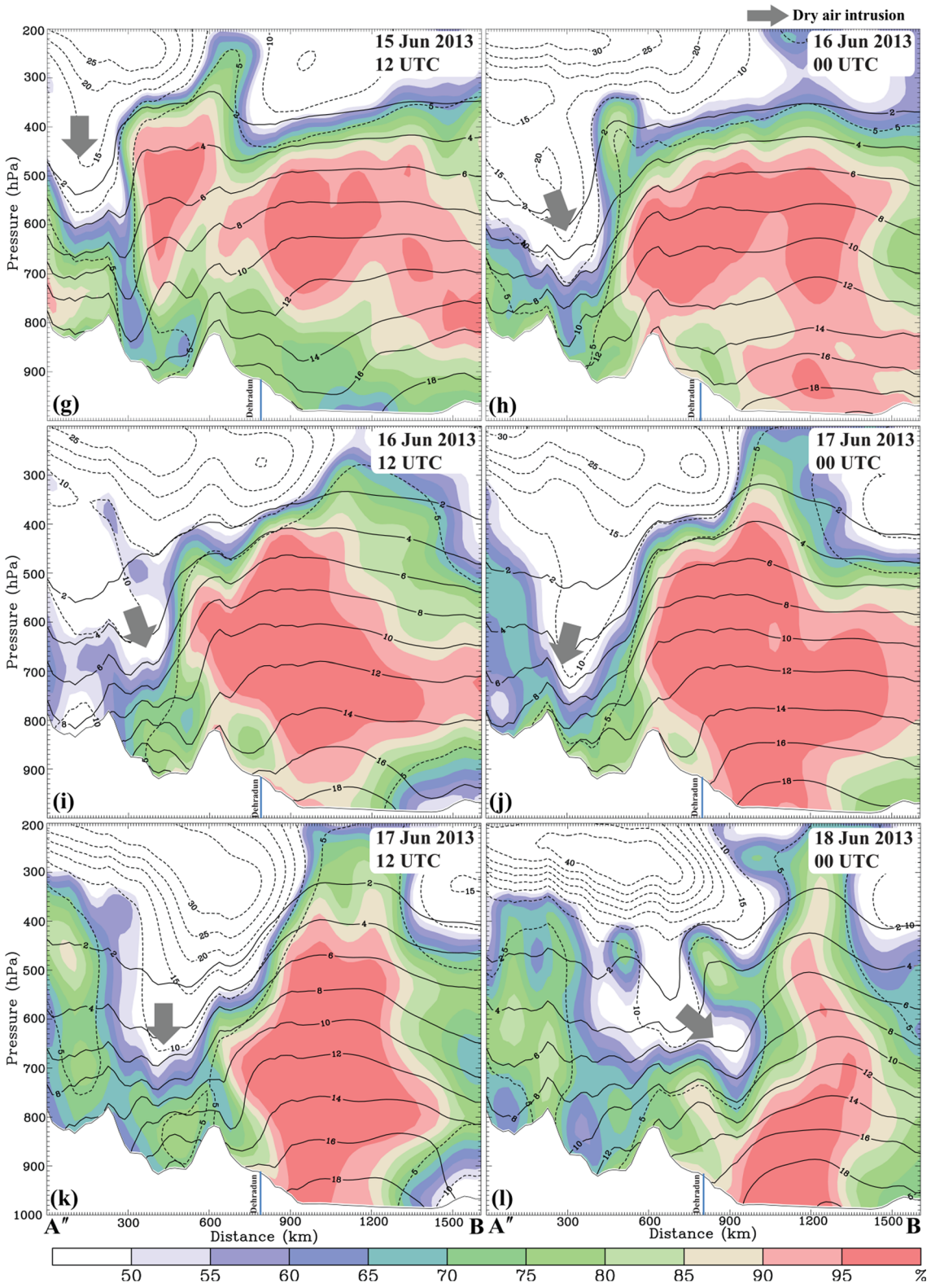

Fig. 5 (continued)

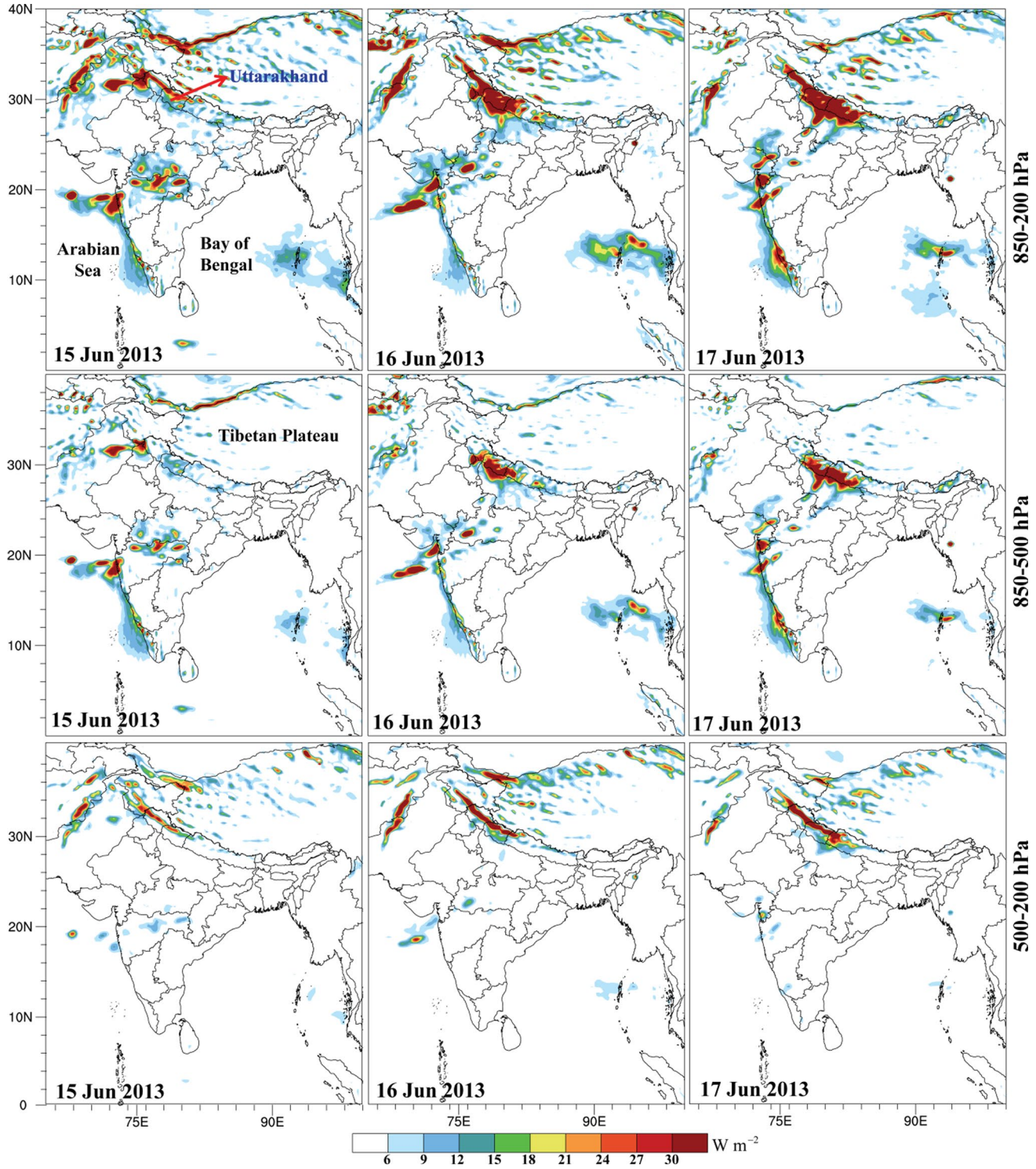

Fig. 6 ERA5 mean column-integrated diabatic heating (W m^{-2}) (top panel) 850–200 hPa (center panel) 850–500 hPa, and (bottom panel) 500–200 hPa diagnosed for the period 15–17 June 2013 (Source: ERA5 reanalysis)

due to greater latent heat release both from convective and stratiform precipitating types (bottom panel of Fig. 6). The heating structure generally reveals that higher [lower] elevations of Uttarakhand, where catastrophic floods were reported appear to come from upper [lower] tropospheric heat sources.

To sum up briefly, mesoscale manifestations of large-scale circulation environment clearly exhibit propensity

of cyclonic vorticity sources from the ISM environment and continued moisture supply toward the Uttarakhand Himalayas during the period 15–18 June 2013. The ISM environment channels the dynamic and thermodynamic scalars through a cyclonically curved conduit trajectory from the Arabian Sea. This trajectory is aligned by evolution of mesoscale ridging patterns from both sides. With additional consequence to wave-breaking events, a vertical conduit of dry air descent emerges in the vicinity of the base of eastward advancing large amplitude upper level trough located to the west of the Uttarakhand Himalayas. This vertical conduit inhibits the penetration of moisture-laden monsoon air further west and northwest of Uttarakhand Himalayas, thereby promoting a quasi-steady potentially unstable environment over the Uttarakhand region, i.e., continued moist convection was preferred at lower elevations from the upslope ascent and semi-organized convection at higher elevations. As the spatiotemporal mesoscale responses of large-scale circulation interactions are critically essential for construing the preferred rain locations, a clear understanding of the finer scale responses to large-scale circulation interactions is imperative for better reasoning of the rapid surge and changes in rainfall intensities during the event period. Therefore, we further examine the fine temporal evolution of PV diagnosed on isentropic surfaces, for better view of the three-dimensional structure of the horizontal flow at mid-levels, in the following.

3 Potential Vorticity (PV) analysis

The PV diagnosed on isentropic surfaces is expressed as follows:

$$\mathrm{PV} = \left(\zeta_\theta + f\right)\left(-g\frac{\partial\theta}{\partial p}\right) = (\text{absolute vorticity}) \times (\text{static stability}), \quad (1)$$

where ζ_θ is the relative vorticity, θ is the potential temperature, g is the acceleration due to gravity, and p is the pressure (Bluestein 1992; Holton and Hakim 2013). The PV is generally positive in the northern hemisphere and is expressed in potential vorticity unit (PVU; 1 PVU = 10^{-6} m^2 s^{-1} kg^{-1} K).

3.1 Rossby wave-breaking (RWB) events

The anticylonic breaking of mid-latitude Rossby waves is typically characterized by low PV air, which folds poleward over the high PV air and this can be clearly noticed at higher isentropic surfaces in the subtropical latitudes (e.g., Homeyer and Bowman 2013). Wave-breaking events seen on the equatorward side of the mid-latitude waveguide tend to generally produce upper level positive PV anomalies or PV streamers (typically seen with large meridional orientation and vertical extension) that can have profound consequences to the downstream extreme weather episodes (e.g., Hoskins et al. 1985; Appenzeller and Davies 1992; Knippertz and Martin 2007; Martius et al. 2008). That is, the RWB serves as vertical conduits for tropical–extratropical mass exchanges, across the Himalayan terrain in this investigation, through which high PV air is injected from higher latitudes into lower latitudes. Vellore et al. (2016) indicated that such isentropic descent of high PV air from high latitudes assist in enhancing the mid-level cyclonic vorticity over the WH region to expedite deeper vertical circulation during the WH extreme rain episodes.

First, a cursory examination of the 300 hPa horizontal wind and geopotential height fields indicate that a barotropic or baroclinically driven wave-breaking signature in its classic form is rather less apparent during the event period (Fig. 7). That is, the RWB signatures exhibited less significant anticyclonic curvature and zonal extent of meridional-negative PV gradients. The RWB generally results in subtropical tropopause folds that can extend much deeper into the troposphere and this scenario potentially can generate an environment for strong convection (see Sawyer 1947; Danielsen 1968; Hoskins et al. 1985). There are two successive wave-breaking signatures noticed just prior to and during the event period. The first RWB signature produced a positive-tilted shortwave trough seen to the east of the Ural Mountains over Russia (within the region 50–60° N, 70–80° E in Fig. 7a) during the period 12–14 June 2013 (see also Fig. 8a, b). The ambient atmospheric environment during this time includes a polar low on the Eurasian Arctic side (see Fig. 7a) protruding into the Siberian Plateau. There is an advancing polar jet (PJ; Fig. 7b) seen along the southern flank of the polar low merging into the nearly straight subtropical westerly jet stream (STJ) along the 40°N latitude belt. Anomalous height excess is also noted between the Mediterranean and the WH region at this time indicating a gradual buildup of anticyclonic circulation over the western part of Eurasia (not shown). The trough in association with STJ amplifies in time through the movement of cold shortwave trough (located on the downstream side of the evolving Eurasian anticyclone) into the long-wave trough. One can clearly notice that the cold wave trough emerges from the northern branch of the PJ drops to south facilitating a trough merger. This strengthens the amplitude of the long-wave trough resulting in a positive-tilted trough axis with the trough base located just northwest of the Uttarakhand region during the period 15–17 June 2013 (Fig. 7b). Strong height gradients seen over the poleward side of the eastern shed

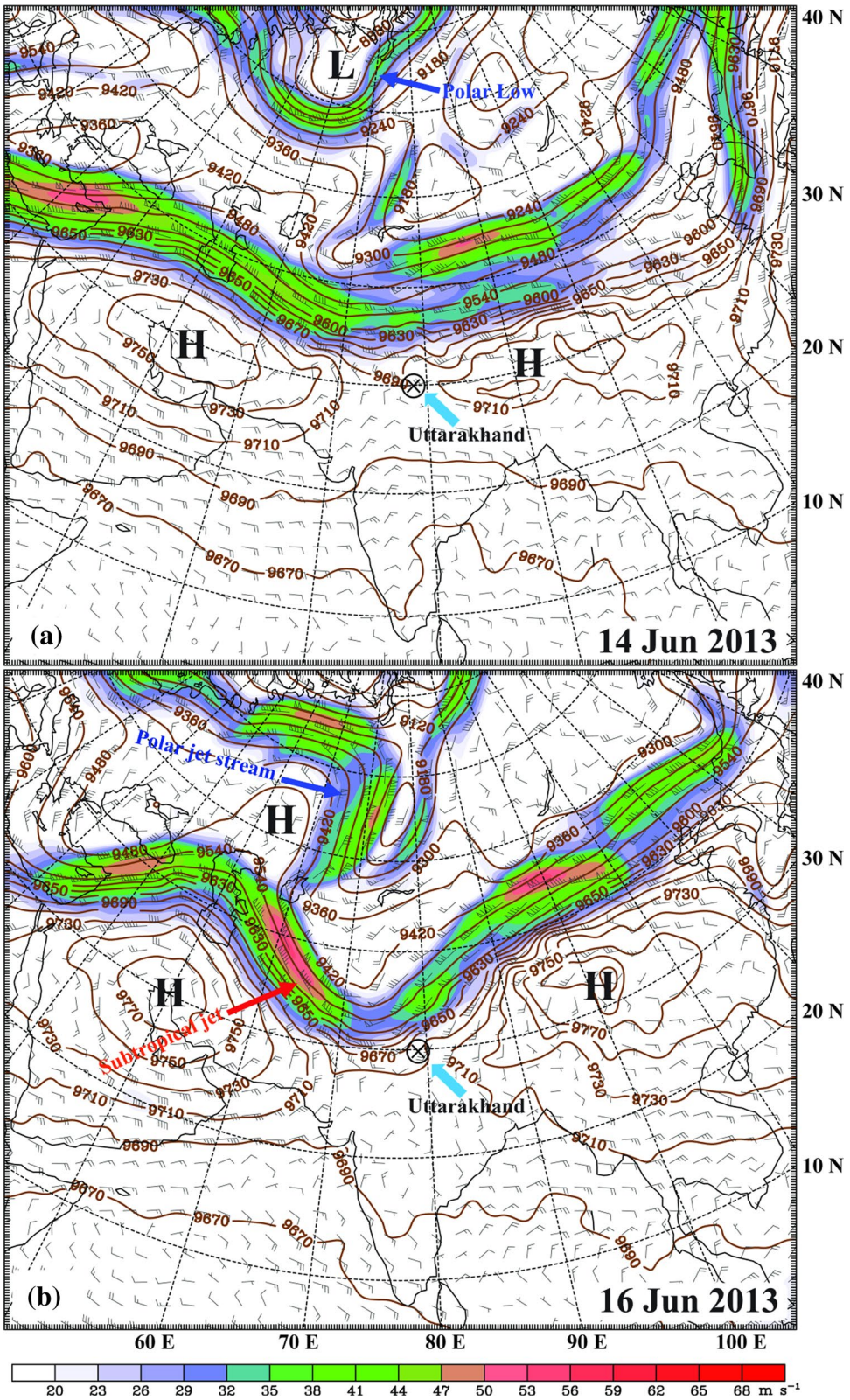

Fig. 7 300 hPa geopotential heights (solid contours; brown) and horizontal winds (isotachs-shaded; full barb = 5 m s^{-1}) on **a** 14 Jun 2013 and **b** 16 June 2013. Polar low, subtropical and polar jet streams are indicated on the figure. Also shown is the location of Uttarakhand (⊗), and low/high (L/H) markers (Source: ERA5 reanalysis)

part of the Tibetan anticyclone at upper levels also lead to generation of mesoscale jetlets poleward of the Uttarakhand region. Thus, the deepening of the long-wave trough is promoted by successive RWB events and PV streamers resulting from these events and their propagation into the ISM region is discussed in the following.

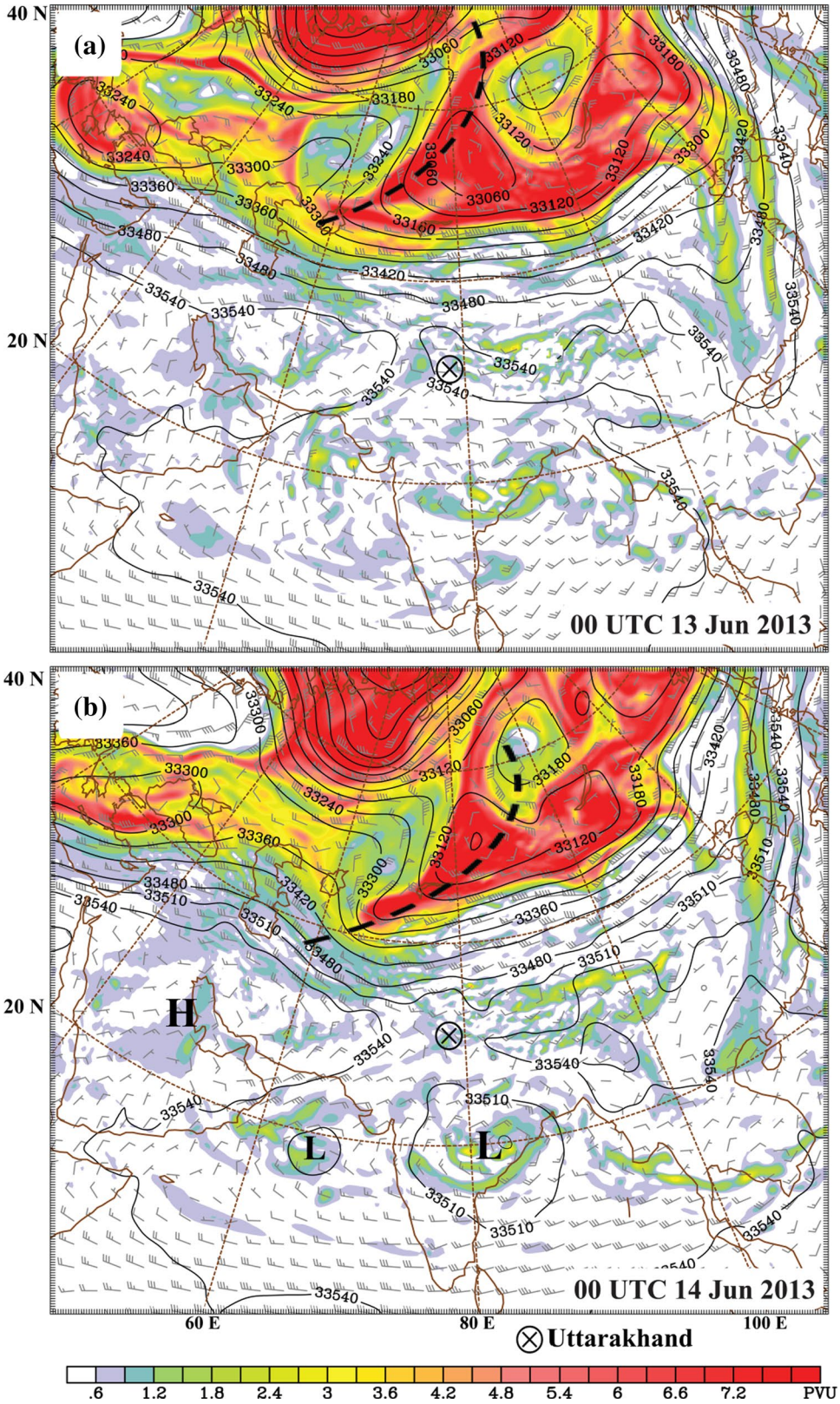

Fig. 8 Potential vorticity (shaded; 1 PVU = 10^{-6} kg^{-1} m^2 s^{-1} K), Montgomery stream function (divided by acceleration due to gravity—contour interval = 30 m), and horizontal winds (full barb = 5 m s^{-1}) diagnosed on the θ = 330 K surface for the period 13–15 June 2013. The upper level trough is indicated by thick dashed lines. Location of Uttarakhand is indicated by ⊗. L, H = Low and High markers (Source: ERA5 reanalysis)

Fig. 8 (continued)

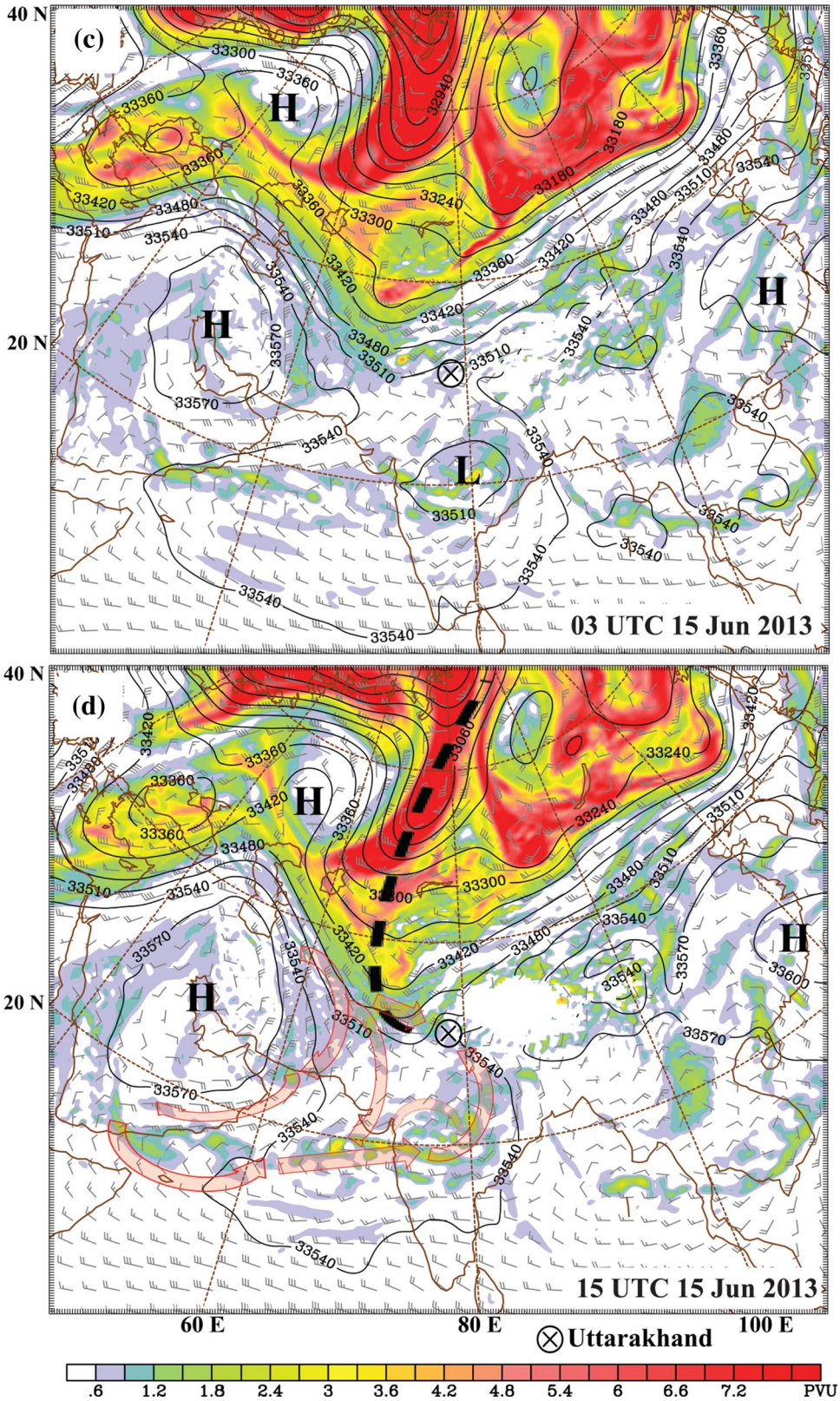

3.2 PV streamers and mesoscale PV structures

Figure 8 shows the planview of PV distribution diagnosed on $\theta = 330$ K surface during the period 13–15 June 2013. This surface generally samples mid-tropospheric (stratospheric) air at low (high) latitudes and is positively sloped from mid-levels in the vicinity of the WH region to about 200 hPa at higher latitudes during this period. As will be seen later, the upper level PV anomaly descends along this isentropic surface and gradually protrudes deeper into the tropical latitudes in time. In response to the underlying topography and diabatic effects, PV streamers split through the upper level fold boundaries resulting in formation of smaller filamentary streamers. These mesoscale filaments from the base of the trough are also found to be effective at and below 330 K isentropic surface (see also Chen 1995; Morgenstern and Davies 1999; Wernli and Sprenger 2007). We refer these PV filaments as mesoscale PV structures detached from the main PV streamer, but embedded within the large-scale circulation. The PV modulations in the vicinity of the WH region can also be attributed to various other factors such as strong wind shear, stretching and shrinking mechanisms as the air traverse over the rugged Himalayan terrain, diabatic processes from convective environment and interactions between the upper and lower level PV anomalies. For this analysis, PV magnitudes larger than 1.5 PVU seen over the extratropical latitudes represent the PV streamers advancing toward the equatorward side. The air streams possessing high PV from the ISM circulation are referred as PV blobs or plumes to contrast the general convention of PV streamers from extratropics (Appenzeller and Davies 1992). The impact of PV streamers on the neighborhood tropospheric environment not only depends on the static stability of the ambient environment in which the streamer is embedded, but also on its size and intensity of the streamer. Also, the dry intrusions of PV anomaly into the troposphere lead to vorticity changes with ascent [descent] ahead of [behind] the PV anomaly (e.g., Hoskins et al. 1985). As will be also seen, the PV streamer during the event period exhibited a larger meridional extent extending from the Arctic region far southward into the tropical latitudes (see also Fig. 8d).

During the first RWB event (13–14 June 2013), there is only little equatorward penetration of PV streamers from high latitudes in association with a shortwave trough induced by the wave-breaking (Fig. 8a, b). These PV streamers excurse into the developing positive-tilted trough along the eastern flank of the anticyclonic air mass located between 60° E and 80° E. Narrow regions of filamentary tropospheric PV streamers (0.6–1.5 PVU) originating from the equatorward flank of the STJ are isentropically advected toward the WH region. However, the zonal extent of tropospheric high PV streamers thin out during the later part of 14 June 2013 in consequence to weakening of the first RWB signal (Fig. 8b, c). More lobes of PV disengage from the base of the trough are advected toward the Uttarakhand region by the mid-level northwesterlies at this time. Another upper level trough from the polar environment emerges from the east of the Ural Mountains, which significantly deepens southward at and later than 15 June 2013 (Fig. 8c, d). This results in greater zonal and meridional extent of PV streamers directed into the westerly trough environment in addition to the PV remnants in the subtropical westerly trough environment from before. The second RWB event commences over the west Siberian Plains (about 60° N and east of 60° E) at this time and the trough axis penetrates much deeper from high latitudes to subtropical latitudes. In other words, significant curvature in the STJ is evident during this period, where the shortwave trough induced by the first RWB event catches up with the long-wave westerly trough resulting in more deepening, increased curvature, and wind speeds across the meridian 70° E (see also Fig. 7). The trough axis gradually becomes more convex downward curved from high latitudes with its base tipping toward the WH region. This curvature also aids greater equatorward extent of mesoscale PV structures from the trough base (or streamer's tip) and advection toward the WH region (Fig. 8d).

Tropospheric high PV plumes (2–3 PVU; higher cyclonic vorticity plumes) from the ISM environment and their transport pathway around the ML are distinctly visible after 12 UTC 15 June 2013 on the $\theta = 330$ K surface (Fig. 9a) and below (not shown). The path of these PV plumes is notably consistent with the METEOSAT-7 cloud imagery (Fig. 4a). It is evident that meso-α scale ML pressure region imbedded in the ISM environment is clearly sandwiched between the evolving ridging pattern from both sides (Fig. 9a). With this ambient setup, there is another branch of filamentary PV structures traversing along the eastern flank of the anticyclonic circulation over the Arabian Peninsula to augment mid-level cyclonic vorticity into the conduit trajectory (see also Fig. 8d). The equatorward moving air along the eastern side of the anticyclonic circulation generally acquires cyclonic vorticity tendency following the conservation of absolute vorticity. The conduit trajectory apparently commences at about 50° E (Fig. 8d) and channels cyclonic vorticity air around the ML. The endurance of this trajectory is assisted by positive vorticity enrichments from the equatorward advancing air and PV enhancements from diabatic heat sources from the ISM environment. Therefore, the aforesaid mesoscale filamentary PV structures from the base of the equatorward advancing trough have two pathways. One is a northwesterly path toward the WH region and other toward the western Arabian Sea (Fig. 8d). In the former one, a backing wind structure is noted in association with cold air advection (and lower θ_e) in the vicinity of the trough base. The latter pathway is associated with deeper swath of northeasterlies down to 700 hPa from the

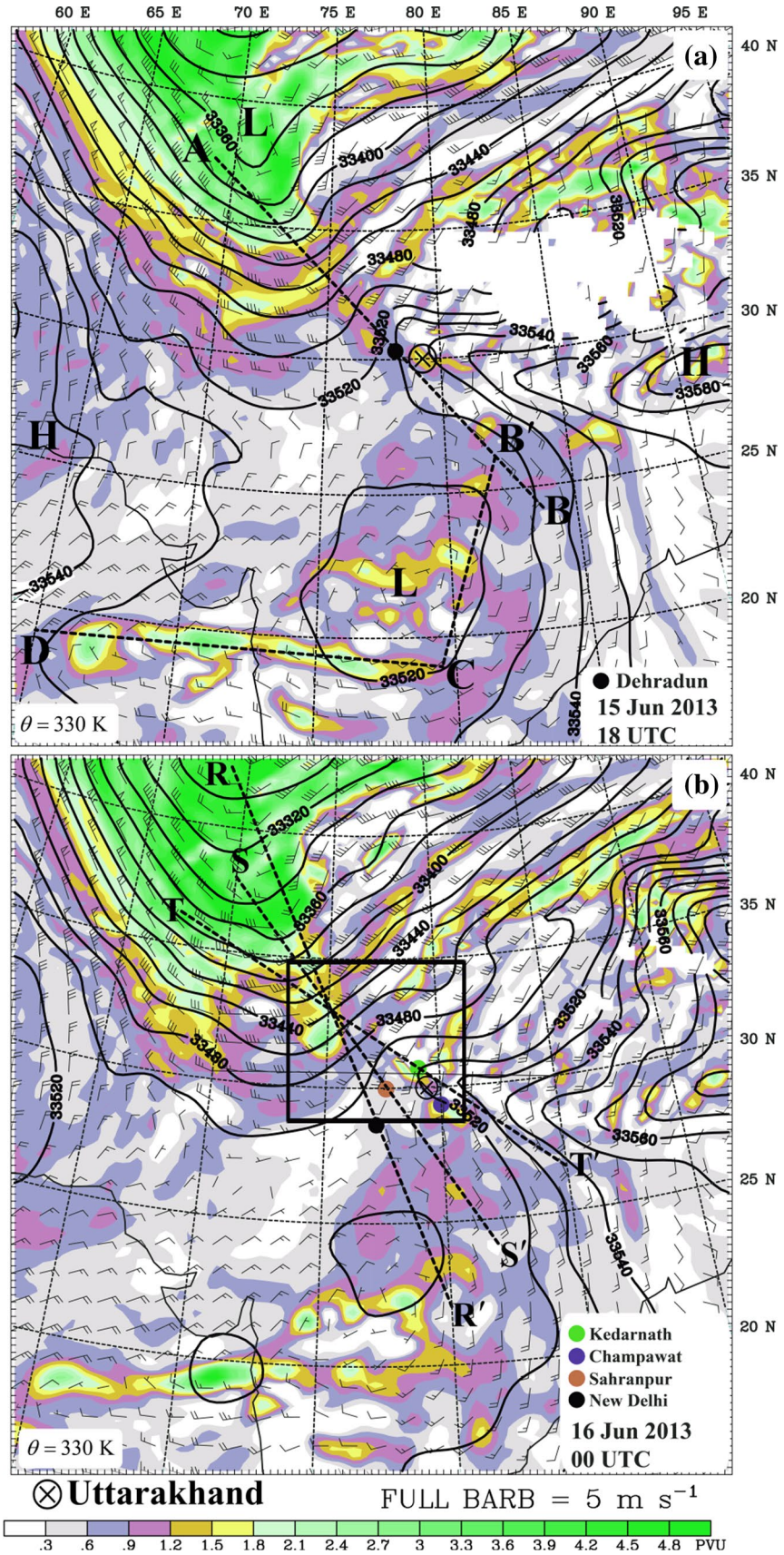

Fig. 9 Potential vorticity (shaded; 1 PVU = 10^{-6} kg^{-1} m^2 s^{-1} K), Montgomery stream function (divided by acceleration due to gravity—contour interval = 30 m), and horizontal winds diagnosed on the θ = 330 K surface for the period 15–18 June 2013. Dashed lines (*A–B*, *B′–C*, *C–D*, *R–R′*, *S–S′*, *T–T′*, *X–X′* and *Y–Y′*) are referenced in the study for the cross-sectional analysis. *L, H* low and high markers (Source: ERA5 reanalysis)

Fig. 9 (continued)

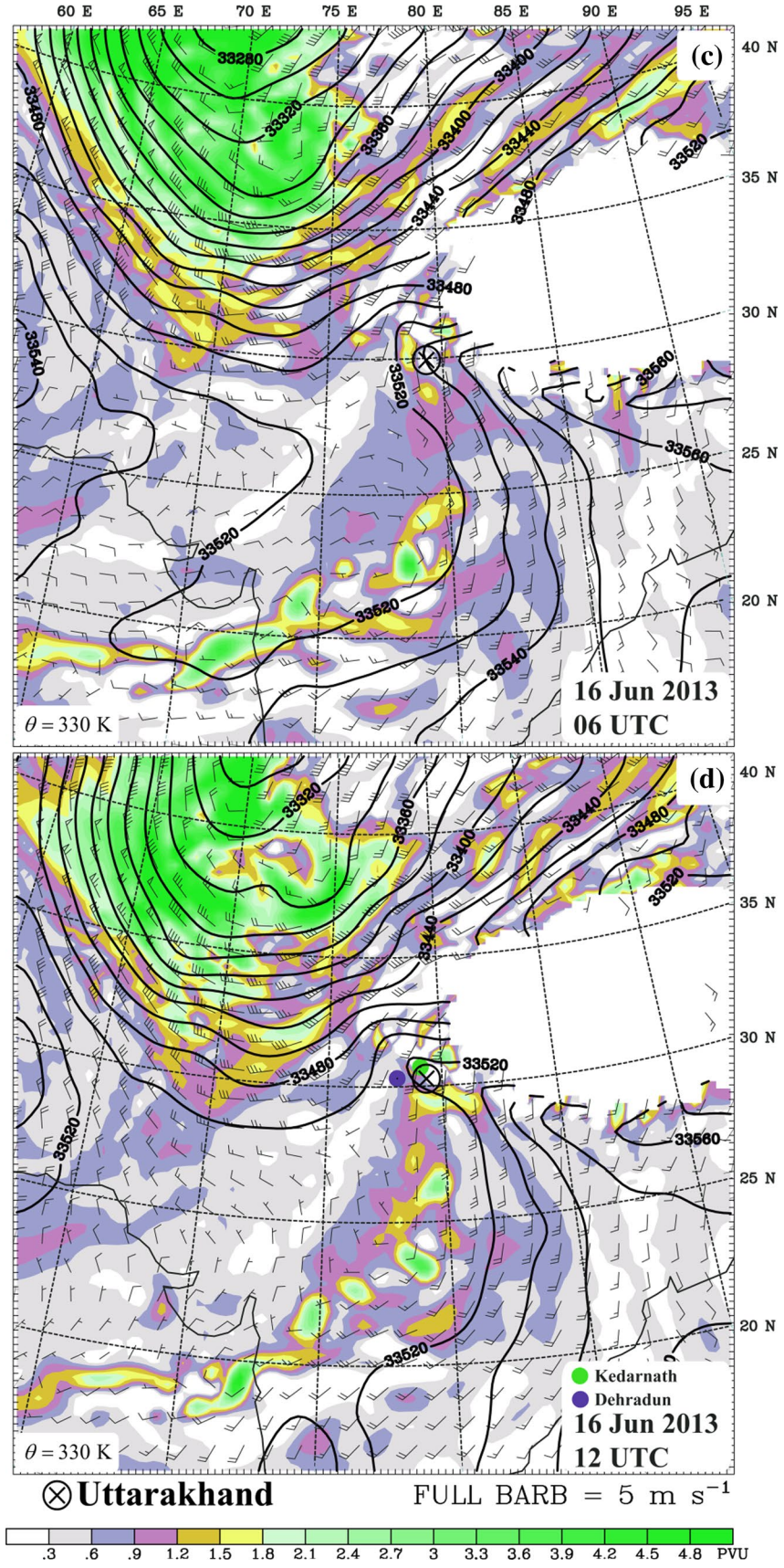

Fig. 9 (continued)

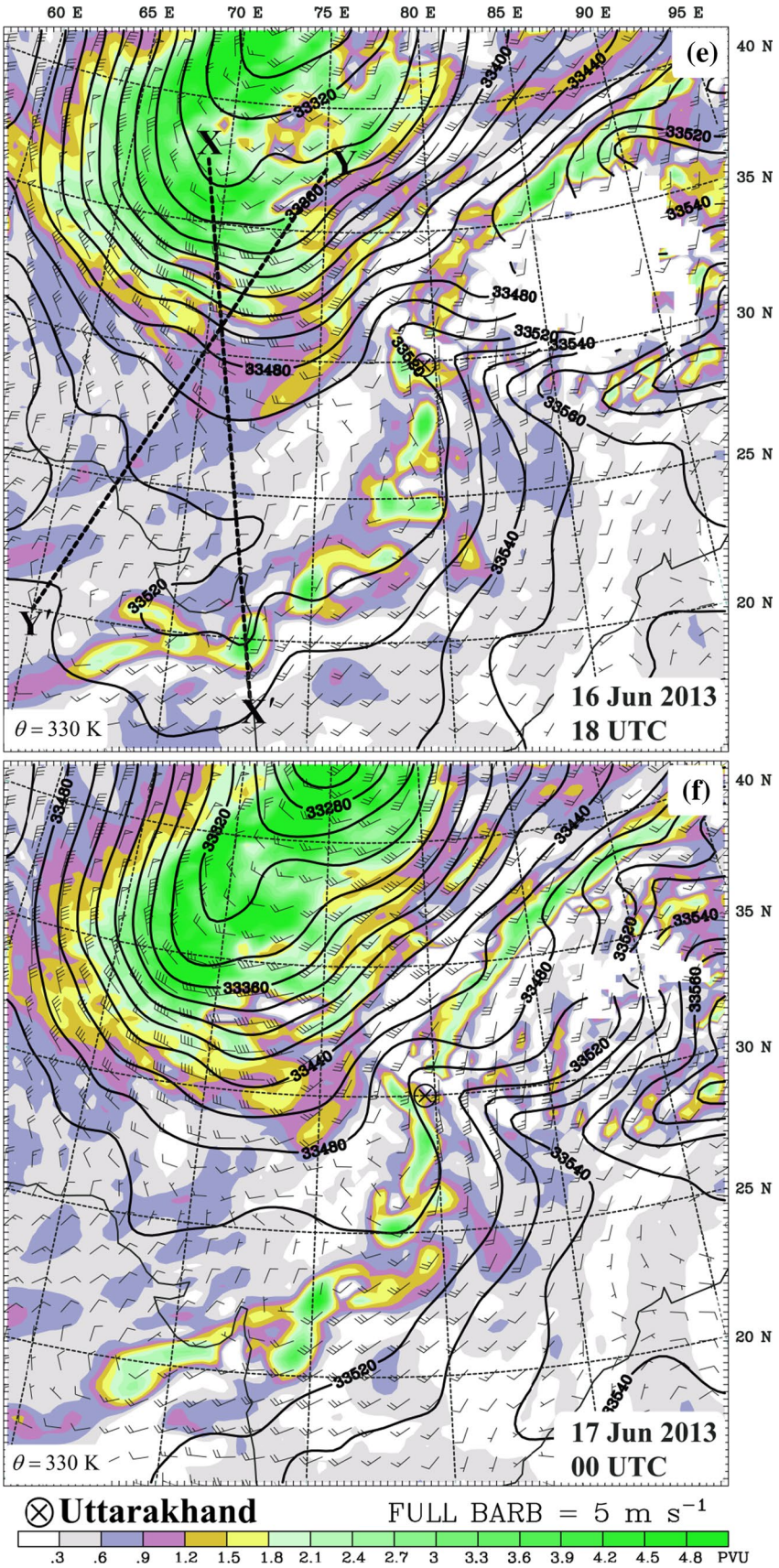

Fig. 9 (continued)

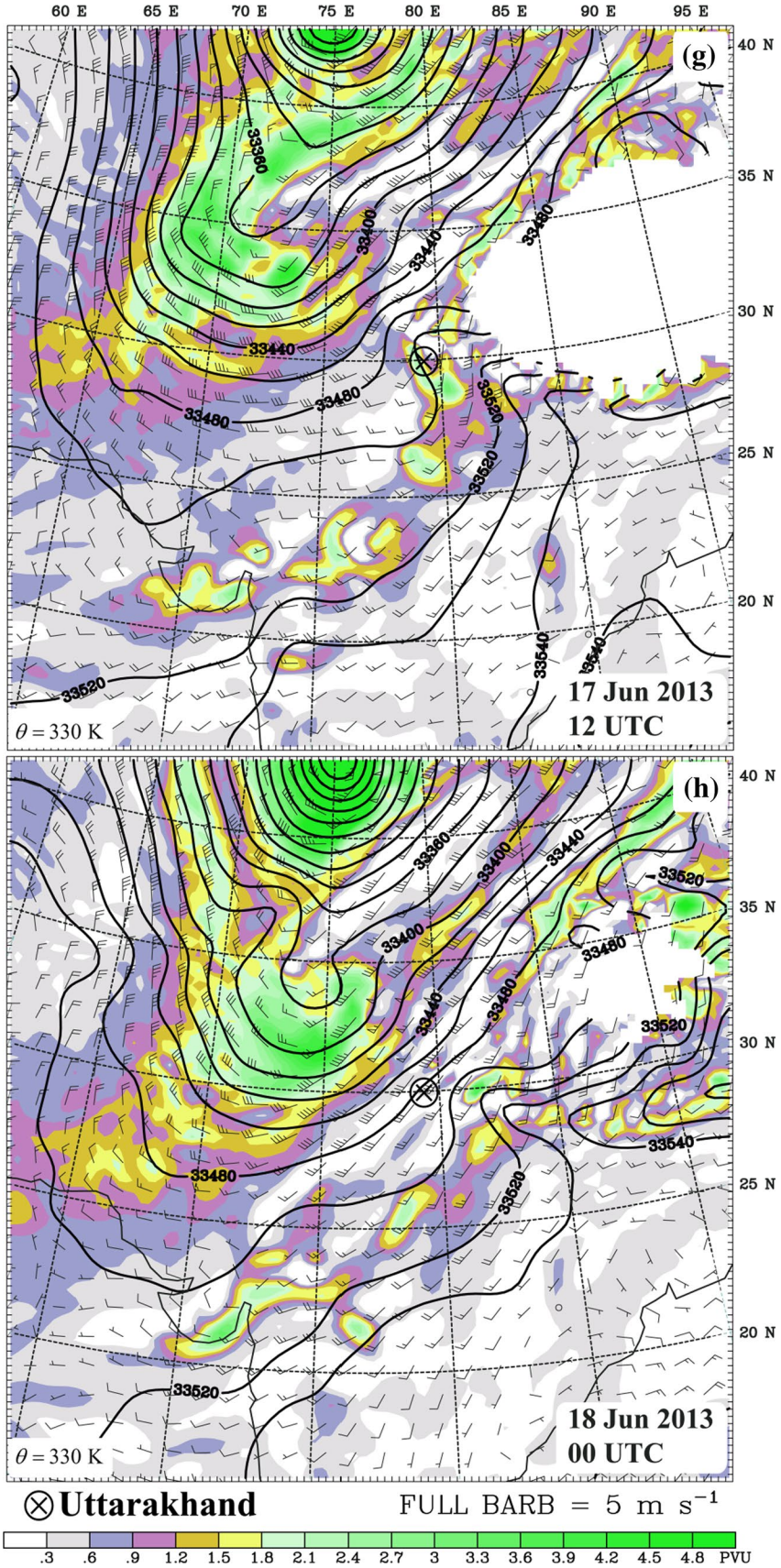

eastern flank side of the strengthening anticyclone centered over the Arabian Peninsula. This circulation setup leads to large shear-induced cyclonic vorticity enhancements within a very narrow region (located just south of 20° N) extending from west to east over the Arabian Sea and also promotes greater westward extent of southwest–northeast orientation of flow around ML (see also Fig. 3g, h). There is also a clear transition from mid-level northerlies turning into westerlies from north to south across this narrow region on 15 and 16 June 2013 (see Figs. 3 and 8d). In short, a quasi-stationary anticyclonic circulation centered over the Arabian Peninsula adjacent to southward penetrating upper level trough deeper into tropical latitudes lends support to continued cyclonic vorticity into the ISM environment from west to east through a narrow conduit trajectory over the Arabian Sea (see Fig. 8d).

Also notice that the PV fluxes from the Arabian Sea are also further augmented by a return flow/PV reinforcements branching around the slowly northward advancing ML (Figs. 8d, 9a–c) during the period 15–16 June 2013. In addition, the evolution of mid-level ridging located to the east of ML apparently not only holds and aligns the conduit trajectory toward the WH region, but also orients the upper level flow to southerly/southwesterly phasing with downstream flow environment of the trough (Fig. 9c, d). In succession with west–northwest migrating ML on 16 June 2013, the deeper cyclonic vorticity plumes embedded within the ISM circulation between $\theta = 310$ and 330 K are advected in an organized manner toward the WH region along the conduit trajectory (see Fig. 9d, e). The mesoscale PV filaments from northwesterly dry PV streamers tend to interact with the southeasterly advection of monsoonal PV plumes approaching the Uttarakhand region during the period 16–17 June 2013 (Fig. 9f). The tropospheric PV enhancements near the foothill region below mid-levels, are in part governed by latent heat release from precipitation and in part due to destruction of upper level PV and interaction between lower and upper level PV anomalies when they come in phase.

Figure 10 shows the vertical structure of horizontal winds, PV, and convective stability examined along the cross-sections *X*–*X*′ and *Y*–*Y*′ (see Fig. 9e for their locations) to further substantiate the equatorward latitudinal extent of mesoscale PV structures from the base of trough. One can notice a PV tongue gradually descending along the 330 K isentrope above a convectively unstable lower troposphere and imminent to enrich the cyclonic vorticity of monsoon flow from the Arabian Sea. With greater cold air advection/backing wind structure in the vertical around the tip of the fold approaching into the northern part of India after 1200 UTC 17 June 2013, the conduit trajectory gradually shifts eastward advecting the monsoon PV plumes to further east of Uttarakhand and western Nepal by the deep-layered southwesterlies from the Arabian Sea (Fig. 9g, h). This also enhances the orographic component of precipitation over this region in association with the flow orientation normal to the Himalayan barrier on the windward side. In addition, monsoonal PV plumes have a tendency of merging with tropospheric PV along the poleward flank of anticyclone located to the east of Uttarakhand region (see Fig. 9h). This is further illustrated using the backtrajectory analysis in the following section.

3.3 Backtrajectory analysis

Figure 11 shows the Lagrangian backtrajectory of air parcels reaching the locations M, N, and O, where M [N] is located over [northwest of] the Uttarakhand region. The parcel trajectories from lower-to-mid troposphere (500–700 hPa) reaching M on 16 June 2013 show a warm–moist conduit trajectory toward the Uttarakhand region through which air parcels of higher cyclonic vorticity (of the order of 10^{-4} s^{-1}) are transported by meridional momentum. Air parcels possessing smaller θ_e (cold/dry air) within 400–600 hPa layer originating from the base of the upper level trough descend to regions of larger θ_e at N at this time. Trajectories reaching the locations slightly northeast of N (and southwest of M) also show similar descending path from aloft and ascending monsoon air trajectories from below 500 hPa (not shown). Therefore, the region located to southwest of M can be potentially envisaged where monsoon and extratropical circulation interactions to occur on finer motion scales. This is also presumably good rationale for torrential rain occurrence over the western part of Uttarakhand during the event period as compared to the eastern part (south and east of M), which is rather more influenced by orographic precipitation enhancements. Further, the anticyclonic trajectory of the parcels from lower and upper troposphere reaching O on 17 June 2013 are strongly influenced by the prevailing high-pressure environment over the Arabian Peninsula and also from the descending fold that is reaching far into the tropical latitudes to favor mid-to-lower tropospheric vorticity enhancements along the southern side of the conduit trajectory.

In short, there is a trail of continued supply of cyclonic vorticity seen along a narrow near circular conduit path (eastern swath extending from northern Arabian Sea to the Himalayan foothills and the western swath from the base of the trough to the northern Arabian Sea; see also Fig. 8d). The conduit path is anchored by ridging patterns on its either sides (see Figs. 3 and 9). The eastern swath of equatorward advancing trough lends support for the horizontal advection of dynamic and thermodynamic scalars (vorticity and moisture) toward the WH foothills, while the western swath appears to promote vorticity sources from the Arabian Sea. The foregoing analysis indicates that there is sustenance in the ambient circulation setup

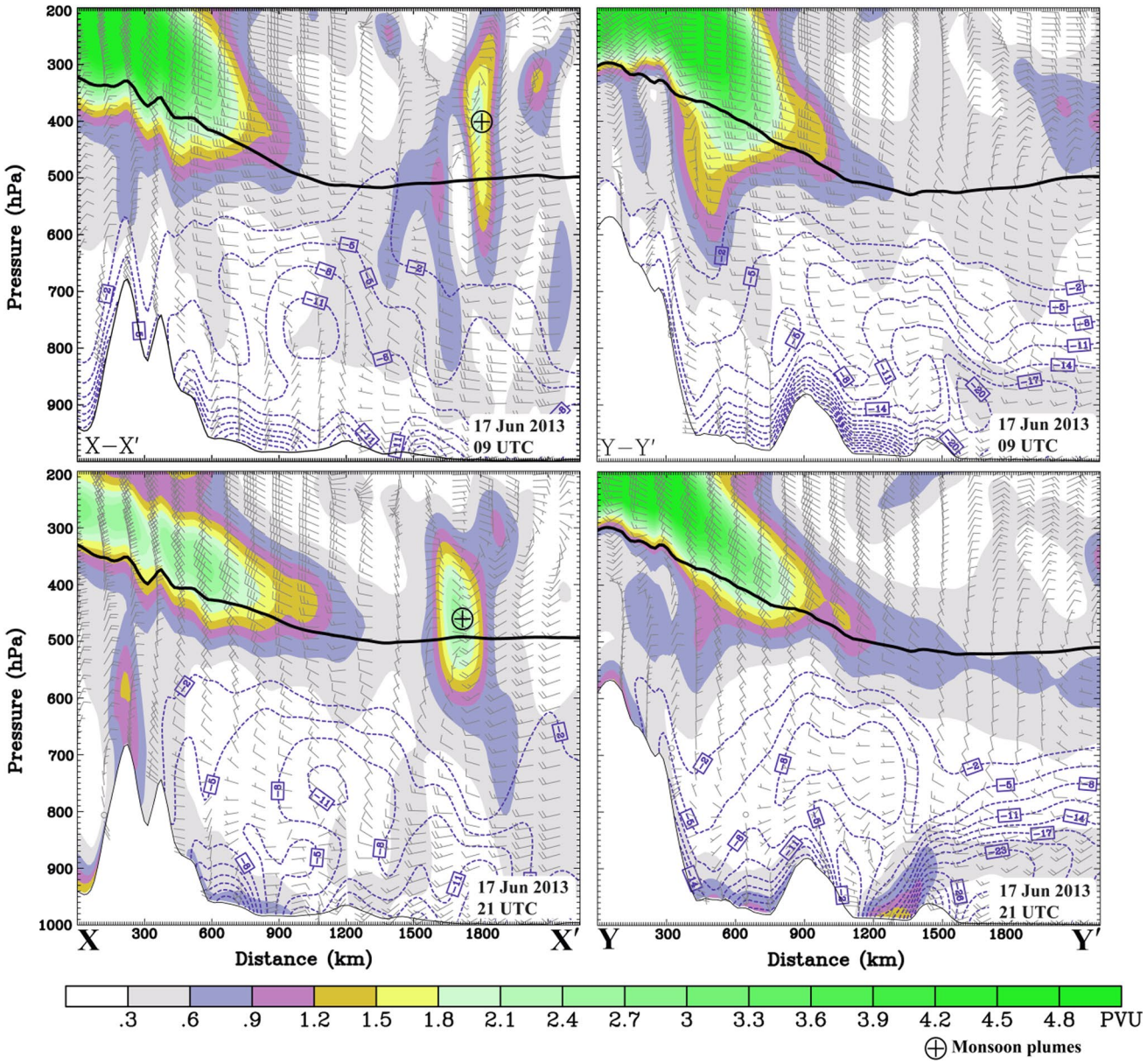

Fig. 10 A cross-section of horizontal winds (full barb = 5 m s^{-1}), potential vorticity (shaded; 1 PVU = 10^{-6} kg^{-1} m^2 s^{-1} K), and convective stability $\left(-\partial\theta_e/\partial p\right)$ (only negative magnitudes are shown in blue-dashed lines; units in K Pa^{-1}) along the cross-sections *X*–*X*′ (left panel) and *Y*–Y′ (right panel) (see Fig. 9e for the locations) at 09 UTC and 21 UTC 17 June 2013. Also the isoline of $\theta = 330$ K is shown by thick solid black line and monsoon PV plumes are indicated by ⊗ (Source: ERA5 reanalysis)

for a few days on either sides of the WH region coupling the northward advancing monsoon circulation and southward intruding extratropical circulation. A two-way interaction mechanism at sub-synoptic periods is conceptualized in the following: (1) sub-synoptic scale precipitation enhancements from the context of mesoscale convergence responses (in the vicinity of M and N in Fig. 11) across the Himalayan barrier in response to monsoon and extratropical circulations, and (2) the far-reaching extratropical circulation acting as a vorticity source to replenish the cyclonic vorticity of monsoon flow which can further assist in event longevity. As deep convective environment often tends to occur on the eastern side of the large-scale upper level PV anomalies with consequences to reductions in static stability (Hoskins et al. 1985), we examine the vertical structure of PV anomaly spanning around the WH region in the following.

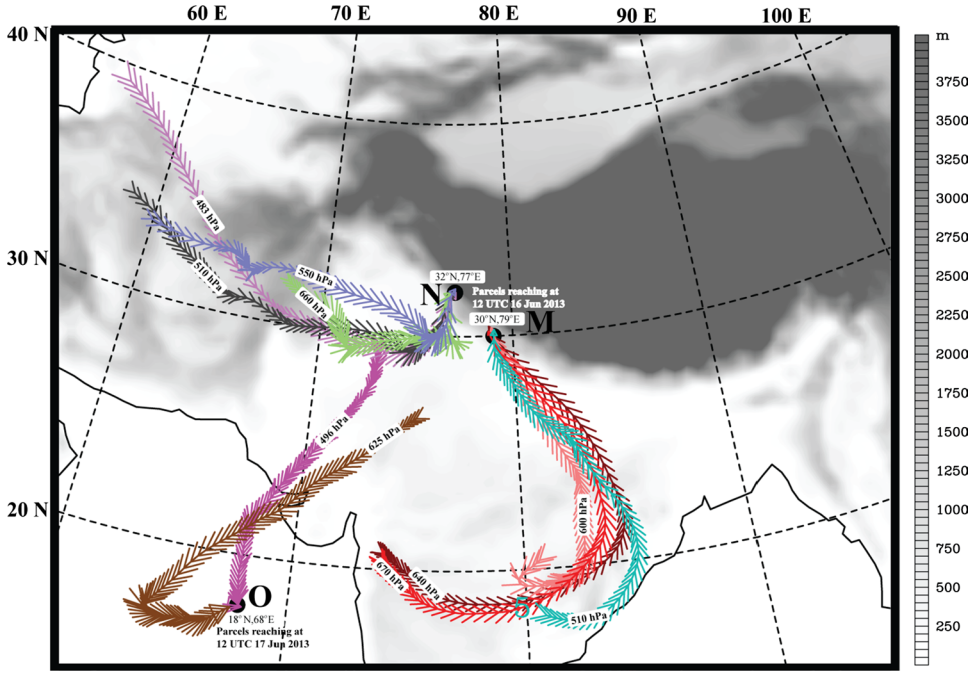

Fig. 11 Lagrangian backtrajectories of air parcels reaching pressure levels (indicated in boxes) at **a** 30°N, 79°E, **b** 32°N, 77°E, and **c** 18°N, 68°E. Parcels reaching M and N start from 00 UTC 14 June 2013 and end at 12 UTC 16 June 2013 (60 h parcel trajectories), and parcels reaching O (85 h parcel trajectories) end at 12 UTC 17 June 2013. Wider (narrower) arrows are indicative of parcel descent (ascent). Shaded regions are terrain elevations shown in meters (Source: ERA5 reanalysis)

4 Mesoscale complement to large-scale circulation interactions

Since there is no unique choice of PV threshold to define dynamic tropopause in tropical and subtropical regions (e.g., Holton et al. 1995; Kunz et al. 2011), 1 PVU isoline is used for tracking the upper level PV anomaly in this study. First, an axial sweep over the longitudes between 60° E and 85° E is carried out about the PV maximum centered approximately at 43° N, 69° E (Fig. 8b) to infer the three-dimensional structure of the flow beneath subtropical fold at upper levels from 14 June 2013. The vertical structure from this sweep generally shows a bi-fold structure of upper level PV anomaly descending down to 600 hPa on the rear flank side of the upper level trough and the leading edge of the PV anomaly (or the streamer's tip) passes right over the $\theta = 330$ K surface. The mesoscale PV filaments detached from the base of the trough exhibit deeper folds in the downstream trough environment with multiple folds along the front flank of the trough bringing the high PV air down to 500–700 hPa. The stratification is generally dry stable (moist unstable) aloft (below 600 hPa) with backing [veering] wind structure evident at the rear [front] flank side of the trough during the 14–15 June 2013 period.

4.1 Subtropical folding and convergence zone

Figure 12 shows a snapshot of the vertical structure of horizontal winds, PV, horizontal wind divergence, and convective stability (vertical gradient of θ_e) and also a planview of PV and horizontal winds on $\theta = 330$ K at 04 UTC 15 June 2013. The fold signature seen to the downstream side of the trough (along *A*–*B*1) profoundly reaches down to 900 hPa destabilizing the lower troposphere over the northern Punjab Plains of the Indo-Pak region together with significant lower-to-mid-tropospheric convergence enhancements in this region (Fig. 12b). The descending fold seen at the upstream side of the trough (along *A*–*A*1) tends to remain quasi-steady with the leading edge located on $\theta = 330$ K surface during the 14–15 June 2013 period (Fig. 12a). The downward advection of air streams into the troposphere through the fold enhances the cyclonic vorticity and ascent at mid-levels and also distinctly separates moist convectively unstable low-level environments that are seen adjacent to the Sulaiman Mountain Range of Pakistan and over the Thar Desert of India (Fig. 12b). The deeper fold generation is indicative of dry air intrusions from aloft to a greater depth with dew point depressions as high as 35 °C seen to the west of this fold. In other words, there is a sharp horizontal gradient in dew point depressions in the vicinity of the descending fold, which distinctly separates the humid environment seen to its east over the Thar Desert (Fig. 12b). The presence of strong PV anomaly at mid-to-lower levels is also indicative of mid-level steepening of lapse rates and vorticity generating ascent ahead in the direction of moving PV maximum.

Therefore, a strong mesoscale convergence zone is generated with significant ascent beneath the detached mesoscale PV structures seen over the regions located to the northwest of the Uttarakhand region (Fig. 12c). Note that this convergence zone is recognized, within the box region shown in Fig. 9b, with deeper vertical extent up to 400 hPa and

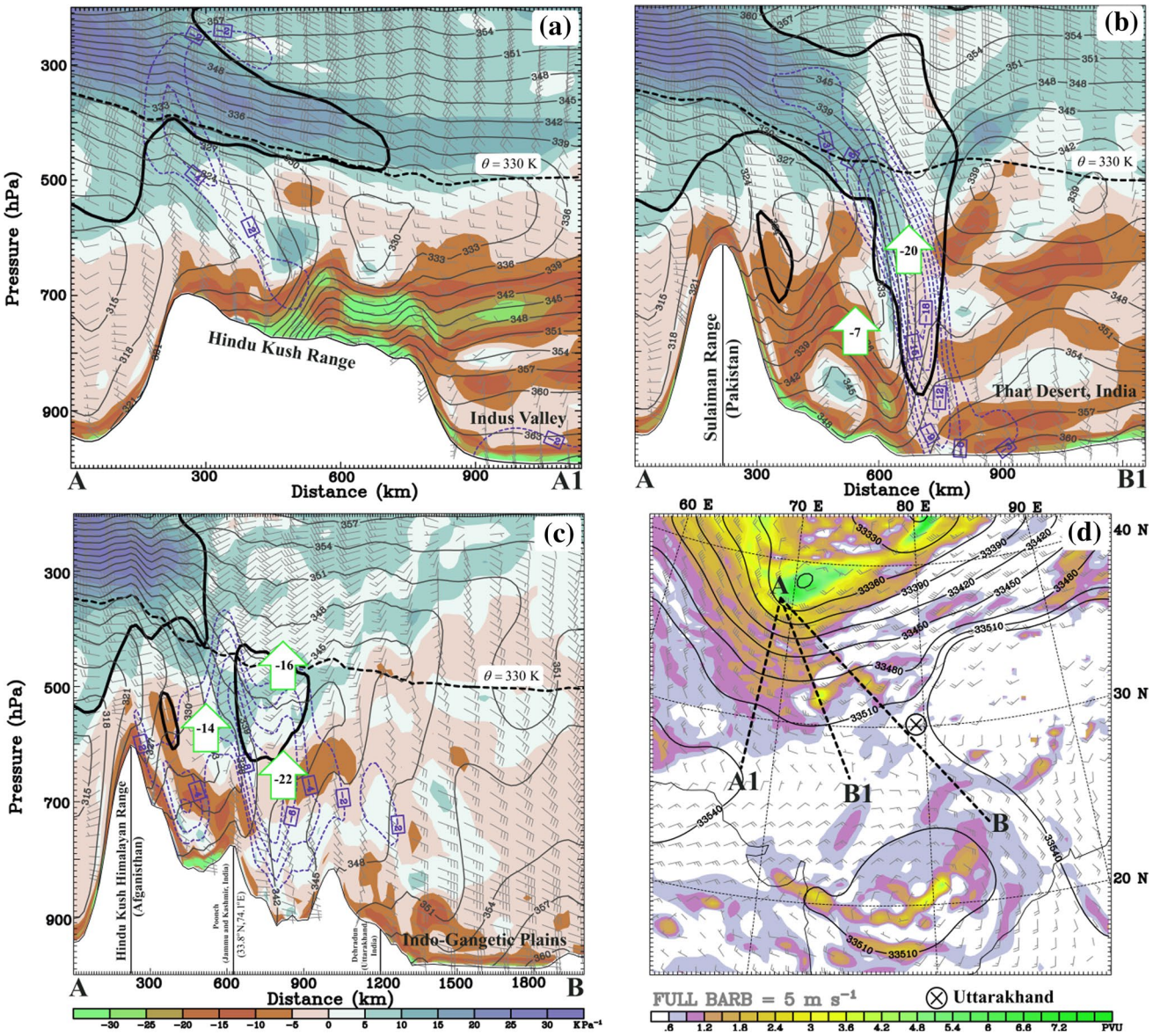

Fig. 12 **a–c** Vertical structure of horizontal winds (full barb = 5 m s^{-1}), θ_e (contour interval = 3 K), horizontal wind divergence (blue-dashed contours; $\times 10^{-5}$ s^{-1}; only negative contours are shown), and convective stability $\left(-\partial\theta_e/\partial p\right)$ [shaded; negative (positive)—unstable (stable) regime] along *A*–*A*1, *A*–*B*1 and *A*–*B*; units in K Pa^{-1}). **d** Potential vorticity (shaded; 1 PVU = 10^{-6} kg^{-1} m^2 s^{-1} K), Montgomery stream function (normalized by acceleration due to gravity; contour interval = 30 m) and horizontal winds diagnosed on the θ = 330 K surface at 0400 UTC 15 June 2013. Vertical arrows indicate ascent (μb s^{-1}). Thick solid and dashed black contours are isolines of 1 PVU and θ = 330 K in **a–c**. Locations of mountain ranges and valleys along the cross-section are indicated on the figure

significant lower-to-mid tropospheric ascent as opposed to the low-level mesoscale convergence zones conjectured by Kotal et al. (2014). Regions of large PV gradients are also noted in areas of significantly sloped tropopause and steeply sloped isentropic surfaces θ = 320 K and 330 K (a steep isentrope dip to a depth of about 200 hPa) within a horizontal distance of 400 km poleward side of the deep fold (Fig. 12b). Warm advection of air dominates the lower troposphere together with a convective unstable environment (negative regions in Fig. 12a–c) underneath the PV anomaly. The upper troposphere is influenced by cold advection of air in the vicinity of the streamer descent indicating an upper level front over this region (Fig. 12b). The disentangling mesoscale PV structures downstream of the trough tend to have isentropic transport pathways between θ = 320 and 330 K surfaces during the 00-12 UTC 15 June 2013 period, while less PV descent below 330 K surface is noted in the upstream side of the trough (Fig. 12a). Over the ISM domain, a PV maximum of about 4 PVU is seen at the center of the ML and diabatic heat-induced PV enhancements are

also noted around its southern flank through which blobs of high PV air are transported from the Arabian Sea between 500 and 700 hPa.

Note that these monsoonal PV blobs are well separated from the descending PV streamer in the vicinity of the WH region at this time (Fig. 12d). Thus, a three-dimensional outlook gives indications of deeper folds/dry air intrusions along the front flank of the upper level trough and potential regions for circulation interactions to occur on finer scales of motion. This is precisely over the region swept across the cross-section *A*–*B* (particularly along the segments of the cross-sections *R*–*R*′, *S*–*S*′, and *T*–*T*′ within the box shown in Fig. 9b). In other words, this is the region where the mesoscale circulation interactions appear to be rather crucial for the confined regions of heavy rainfall over the Uttarakhand region in conjunction with a persisting dry air shielding from deeper folds located to its west. Therefore, the vertical structure of circulation evolution and thermodynamic variables is discussed in the following.

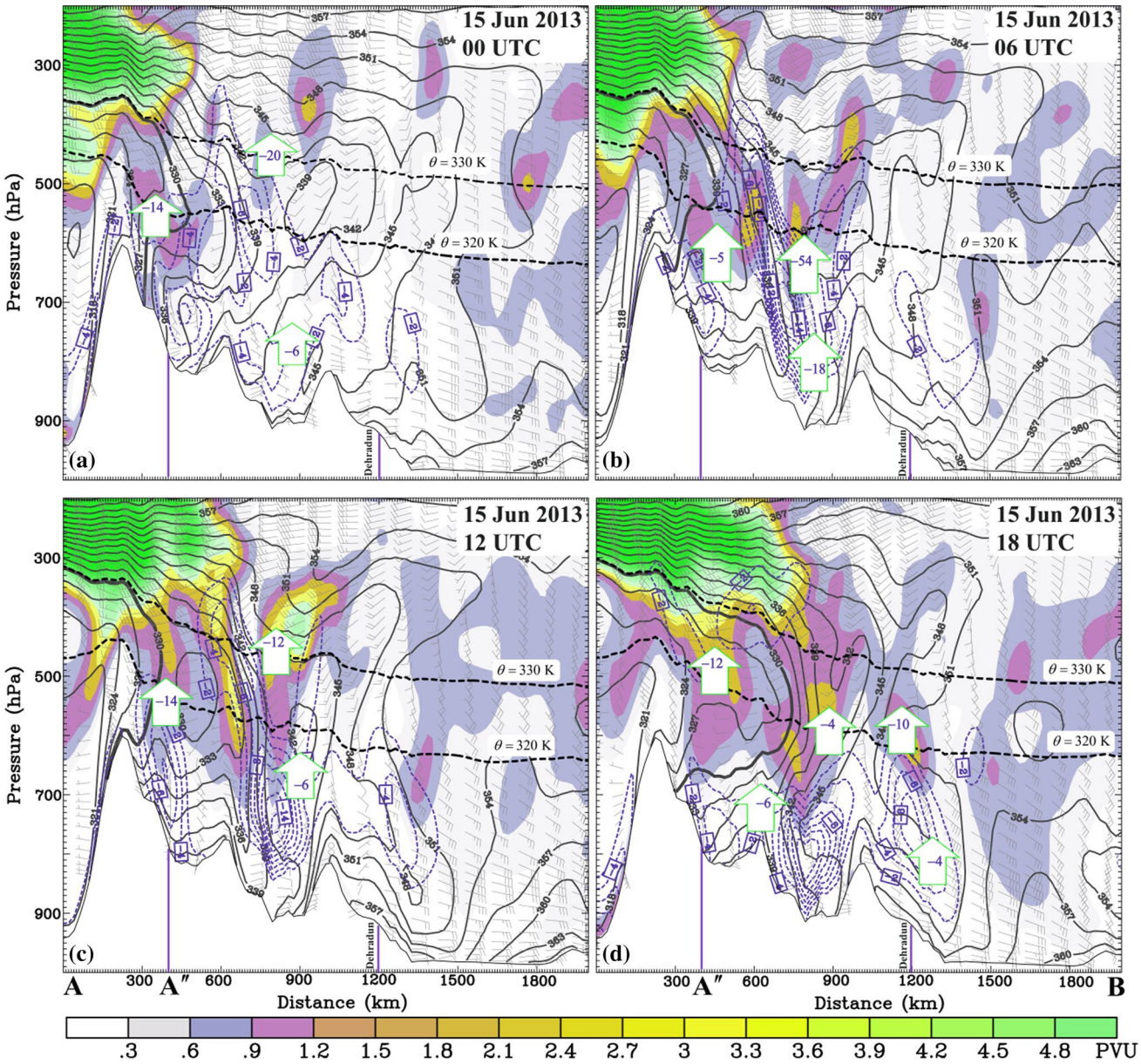

Fig. 13 Vertical structure of potential vorticity (shaded; 1 PVU = 10^{-6} kg^{-1} m^2 s^{-1} K), equivalent potential temperature θ_e (contour interval = 3 K), horizontal winds (full barb = 5 m s^{-1}) and horizontal wind divergence (blue-dashed contours; $\times 10^{-5}$ s^{-1}; only negative part is shown) along the cross-section *A*–*B* (see Fig. 9a) during the 15–17 June 2013 period. Locations of Dehradun and Kedarnath in Uttarakhand are indicated along the cross-sections. Also the isolines of θ = 320 and 330 K (θ_e = 330 K) are shown by thick (solid) dashed lines. Monsoon PV plumes are indicated by ⊕ Ascent (μb s^{-1}) is shown by vertical arrows. (Source: ERA5 reanalysis)

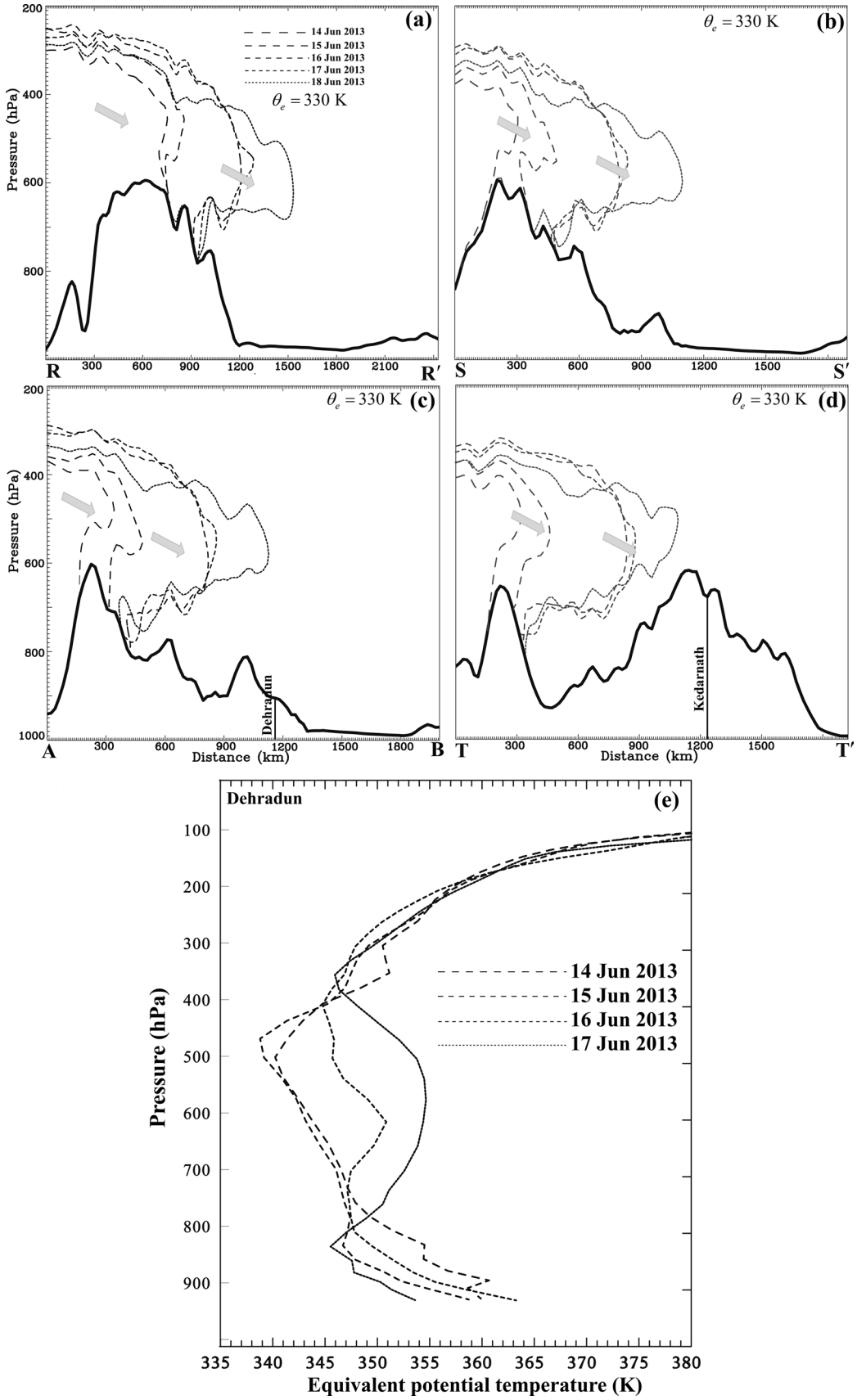
(a)
14 Jun 2013
15 Jun 2013
16 Jun 2013
17 Jun 2013
18 Jun 2013
θ_e = 330 K
Pressure (hPa)
R
R′
(b)
θ_e = 330 K
S
S′
(c)
θ_e = 330 K
Dehradun
A
B
Distance (km)
(d)
θ_e = 330 K
Kedarnath
T
T′
Distance (km)
Dehradun
(e)
14 Jun 2013
15 Jun 2013
16 Jun 2013
17 Jun 2013
Pressure (hPa)
Equivalent potential temperature (K)

◂**Fig. 14** **a–d** Vertical structure of the $\theta_e = 330$ K isoline along the cross-sections *R–R′*, *S–S′*, *T–T′*, and *A–B* (see also Fig. 9a, b for the locations) during the 14–18 Jun 2013 period. Arrows indicate direction of low θ_e advection toward the northern part of India. **e** Vertical profiles of at Dehradun for the period 14–17 Jun 2013. Locations of Dehradun and Kedarnath are shown on the figure (Source: ERA5 reanalysis)

4.2 Vertical structure within the mesoscale interaction zone

Figure 13 shows the vertical structure of PV, θ_e, horizontal winds, horizontal wind divergence, vertical motion, and convective stability along the northwest–southeast oriented cross-section *A–B*, which passes through Dehradun, Uttarakhand (see Fig. 9b for the location) on 15 June 2013. Southeastward progressing larger PV from the upper level PV anomaly are evident along *A–B* with the PV descent down to 700 hPa over the regions southeast of the Hindu Kush Mountain range of Afghanistan (first mountain peak along *A–B*; see also Fig. 12c for the location) early on 15 June 2013. Also notice the gradually intensifying mesoscale convergence zone (of the order of 10^{-4} s^{-1}) in time over northern part of India along the front flank of the trough resulted from the tropospheric destabilization through descending folds (Fig. 13b–d). The deeper convergence zone is clearly evident on a horizontal scale of a few hundreds of kilometers over the region across the cross-section *A–B*. A similar scenario is also noted along the segment parts of the other cross-sections shown within the box region in Fig. 9b (not shown). The destabilization significantly promotes convectively unstable lower-to-mid tropospheric environment juxtaposed with significant ascent in the region northwest of Uttarakhand. The regions of ascent imply the regions promoted by strong positive PV advection, i.e., advection of higher PV toward lower values by horizontal winds.

Significant positive PV advection is noticed aloft and a scenario emerges consistent with Hoskins et al. (1985) who indicated that circulation gets unbalanced (ageostrophic), when a PV anomaly moves over to a region and intense warm advection aloft occurs in the areas of large positive PV advection coincident with areas of ascent at mid-levels (Fig. 13d). The low-level moisture-laden monsoon air parcels are advected toward the foothill region and acquire greater tendency of ascending or upgliding along the isentropes, while approaching toward the PV anomaly, which also facilitates deeper moist convective environment over Uttarakhand and the regions to its northwest. This is also evidenced in the vertical structure of θ_e, where relatively drier column of air within the 800–400 hPa layer gradually turns into moist column with the approaching monsoon air at Dehradun (Fig. 14e) due to positive [negative] advection of θ_e by the monsoon [relatively drier subtropical] winds. Also notice that time evolution of the vertical structure of isoline $\theta_e = 330$ K indicates that dry air penetration toward the region of convergence is rather three-dimensionally consistent from the west (Fig. 14a–d).

4.3 Advective interactions

It is noted that horizontal PV advection by monsoon winds is apparently pronounced at higher elevations at Kedarnath during the 15–17 June 2013 period, i.e., there is a greater tendency of phasing or interaction between the upper and lower level PV advection at higher elevations of Uttarakhand during the entire event period (Figure not shown). Briefly, the advective interactions of PV and moisture between extratropical and monsoon air are more (less) significant at higher (foothill) elevations of Uttarakhand on 15 June 2013. The fold significantly drops down below to mid-levels and holds the prevalence of a strong convergence zone within the box region (Fig. 9b) and a greater vertical alignment of positive advection of scalars is realized throughout the entire day on 16 June 2013 (Fig. 15). The synchronization of positive PV advection by monsoon winds and positive PV advection aloft at lower foothill elevations is clearly evident from 06 UTC 16 June 2013 (Fig. 15a). The positive moisture advection over northern part of India is also more pronounced and seen to penetrate much deeper to about 400 hPa and above during this time. However, its vertical extent is constrained in time by northeastward penetration of the fold into the region (Fig. 15b).

Figure 16 shows the vertical structure of PV, θ_e, horizontal winds, horizontal wind divergence, and ascent along the cross-section *A″–B* (see Fig. 5d for the location) during the 16–17 June 2013 period. The rising magnitudes of PV over the WH region during this period can be attributed to the mesoscale interactions with descending PV structures from aloft together with the latent heat release from precipitation over the Uttarakhand region. The monsoonal PV blobs (marked by ⊕) from lower-to-mid troposphere approaching the foothill region through the conduit trajectory (*A–B–C–D*; see Fig. 9a for the location) are strongly interacting with the subtropical PV descent from aloft on 16 June 2013. This cyclonic vorticity interaction apparently tends to intensify the convergence zone and associated ascent over the Uttarakhand region (Fig. 16). Further, it is noteworthy to mention here that the aforesaid strong phasing periods of low-level monsoon and upper level extratropical flows commencing from 06 UTC 16 June 2013 (Fig. 15a) are also coincident with rapid surge in observed rainfall intensities to as high as 30–40 mm h^{-1} over the western districts of Uttarakhand [cf. Figure 1 of Ranalkar et al. (2016a)]. There is a sustained period of observed rainfall intensities greater than 20 mm h^{-1} on 16 June 2013. A slow eastward progression of dry air shielding located to the west of Uttarakhand region during the 15–17 June 2013 period allows

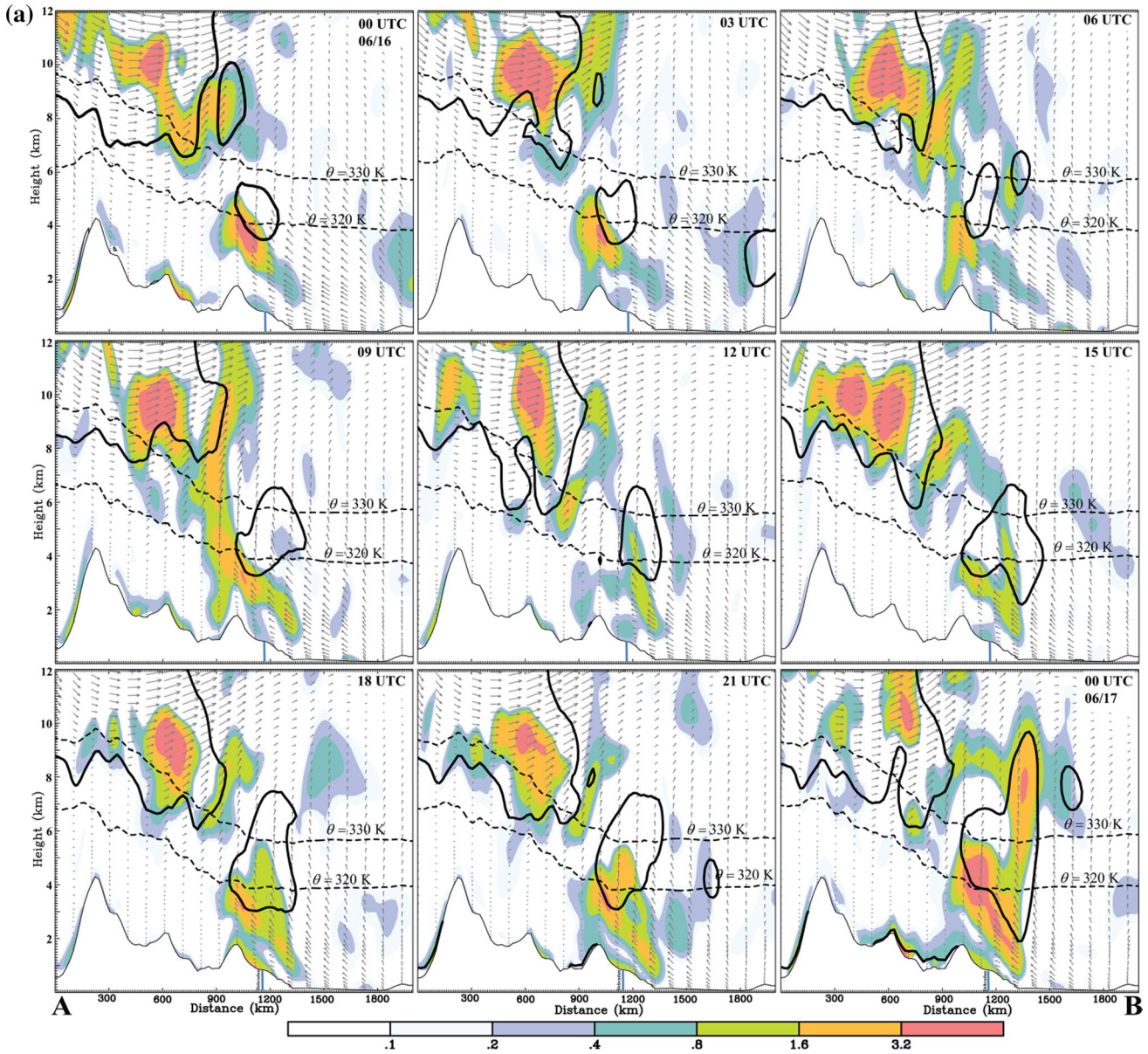

Fig. 15 **a** Vertical structure of PV advection by horizontal winds (shaded; $\times 10^{-4}$ kg^{-1} m^2 s^{-2} K—only positive advection is shown), horizontal winds (Max vector = 40 m s^{-1}) along the cross-section *A*–*B* (see Fig. 9a for the location) at 3-h intervals on 16 June 2013 Also isoline of 1 PVU (θ = 320 and 330 K) is shown by thick solid (dashed) line. Location of Dehradun in Uttarakhand is shown in the figure (Source: ERA5 reanalysis). **b** Vertical structure of moisture advection by horizontal winds (shaded; $\times 10^{-4}$ g kg^{-1} s^{-1}), horizontal winds (maximum vector = 40 m s^{-1}) along the cross-sections *A″*–*B* (southeastern part of the cross-section *A*–*B*; see Fig. 5d) on 16 June 2013. Dashed lines are the dew point depressions (°C). Location of Dehradun is shown in the figure (Source: ERA5 reanalysis)

the moisture-laden monsoon air streams penetrating into the western part of Uttarakhand favoring an intensive convective environment and rains. The rapid eastward progression of the aforesaid dry air shielding after 17 June 2013 results in precipitation reduction over the western districts of Uttarakhand (Fig. 15b). Further, eastward drifting of the conduit trajectory by the southeastward advection of cold/dry subtropical air from the descending fold (see Fig. 9g, h) favors orographic precipitation enhancements over the eastern side of the Uttarakhand and western Nepal. A cross-section passing through the station (a slight tilt of eastern end of *A*–*B* passing through Champawat—see Fig. 1) also indicated stronger convergence zone with PV interactions in addition to favored orographic uplift over this region (not shown). To summarize, the rapid rise in precipitation intensities during the sub-synoptic periods on 16 June 2013 is in conjunction with strong synchronization of scalar advective interactions on mesoscale in addition to orographic effects

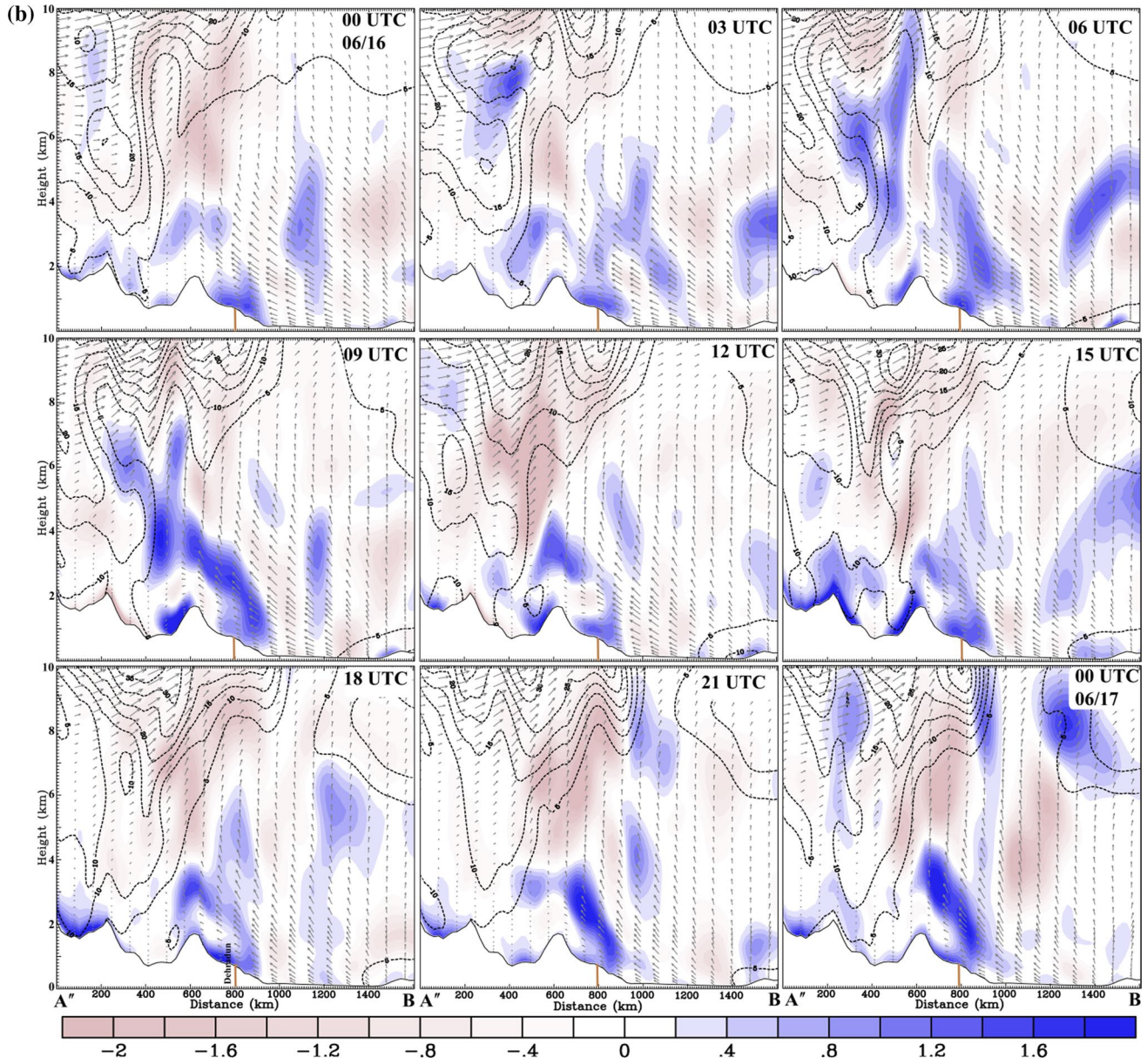

Fig. 15 (continued)

over the Uttarakhand Himalayas. The precipitation consequences over the western and eastern districts of Uttarakhand appear to significantly come from orographic influences with greater possibilities of quasi-static convective environment on 15 and 17 June 2013.

5 Summary

This study revisits our earlier work to further augment the understanding of finer scale dynamical processes associated with the extremely heavy rainfall ($\geq$ 240 mm day^{-1}) event occurred over the North Indian state of Uttarakhand located in western Himalayas (WH) during the 15–18 June 2013 period. Various studies hitherto reported about this event largely associated the causes for extreme rainfall to orographic lifting of moist large-scale monsoon flow and large-scale circulation interactions across the Himalayan barrier. The circulation interactions are associated with the northward advancing low-level Indian summer monsoon (ISM) and southward advancing large amplitude mid-latitude westerly troughs. Nonetheless, there is a large ambiguity in the finer scale understanding of the causal mechanisms. In particular, on the reasoning behind the persistence of intense rainfall with significant spatiotemporal variability for a few consecutive days over a confined region of Uttarakhand

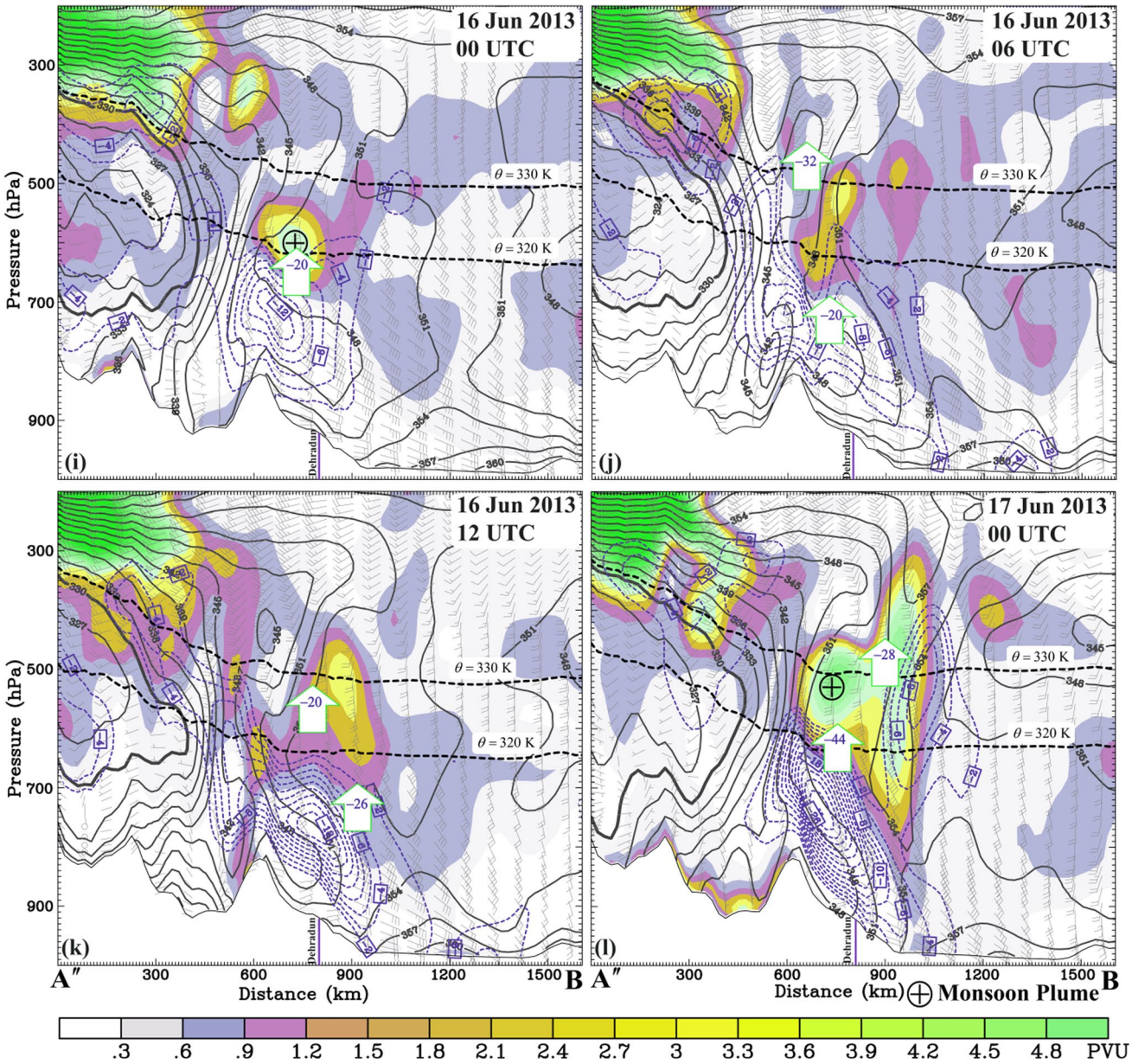

Fig. 16 Vertical structure of potential vorticity (shaded; 1 PVU = 10^{-6} kg^{-1} m^2 s^{-1} K), horizontal winds (full barb = 5 m s^{-1}) and horizontal wind divergence (blue-dashed contours; $\times 10^{-5}$ s^{-1}; only negative part is shown) along the cross-section *A″–B* (southeastern part of the cross-section *A–B*; see Fig. 5d) during the 16–17 June 2013 period. Locations of Dehradun and Kedarnath in Uttarakhand are indicated along the cross-sections. Also the isolines of $\theta = 320$ and 330 K ($\theta_e = 330$ K) are shown by thick dashed (solid) black lines. Monsoon PV plumes are indicated by ⊕ and green arrows on the figure indicate vertical *p*-velocity (μb s^{-1}) maxima (Source: ERA5 reanalysis)

Himalayas. This study investigates this issue using finer spatiotemporal analyses from the latest ERA5 reanalysis product focusing on the sub-synoptic/mesoscale complement of large-scale circulation interactions during the event period.

Examination of sub-synoptic circulation analyses reveals that there is a continuous propensity of positive vorticity sources from the ISM environment during the event period, which is channeled toward the WH region to enhance the longevity of the precipitation event. This channel is a narrow quasi-steady curved horizontal conduit in the lower-to-mid troposphere embedded within the ISM environment whose curvature is regulated by the mesoscale evolution of mid-level ridge pattern adjacent to the right of ISM environment. There is a vertical conduit of dry air descent from the downstream side of upper level westerly trough inhibiting the moisture-laden monsoon air penetrating further west

and northwest of the Uttarakhand advocating a persisting potentially unstable moist environment over the Uttarakhand region. A vast latitudinal extent of this vertical conduit is also recognized to the west of ISM environment in consequence to equatorward evolving upper level potential vorticity (PV) anomaly, which steadily endures the aforesaid horizontal conduit path. Further, the equatorward sequestered mesoscale potential vorticity (PV) structures emerging from the upper level PV anomaly renders pathways for vorticity sources during the event period. One from the base of the trough culminating into longer horizontal conduit path from the western Arabian Sea lending perpetual cyclonic vorticity support to the ISM environment. The other is a northwesterly pathway through the vertical conduit from right flank of the trough to promote a sustained environment of deeper mesoscale convergence zone and strong ascent over the WH region. A schematic of the processes discussed in this study is briefly shown in Fig. 17.

This deeper convengence zone is realized as the potential region for monsoon and extratropical circulation interactions to occur on mesoscale, where there is a vertical synchronization or phasing of positive advective interactions of PV (and moisture), which is clearly noticeable at higher elevations (e.g., Kedarnath) during most of the event period. Such synchronization is less conspicuous at foothill elevations (e.g., Dehradun) on 15 June 2013, which suggests the traits of orographically induced precipitation component for the enhanced foothill rainfall at this time. But, there is a significant vertical alignment of positive advection of PV and moisture noted on 16 June 2013, which is apparently coincident with the rapid surge in observed rainfall intensities along the foothill elevations of western side of Uttarakhand Himalayas. Although it is implied that there is a sustained PV source from continued precipitation and associated latent heating over the WH foothill region, the PV enhancements over the WH region and their interactions with the upper level PV anomaly are clearly discernible to support the vertically aligned interactions on 16 June 2013. The persisting sub-synoptic periods of the aforesaid vertically aligned interactions can be attributed to the expeditious rise and sustenance of heavy rainfall intensities. The aforesaid mesoscale convergence zone and the pattern of monsoon–extratropical PV interactions move eastward after 17 June 2013 in consequence to eastward progression of the upper level PV anomaly causing an eastward drift in the conduit trajectory carrying vorticity sources from the ISM region. This causes increased (reduced) rainfall intensities over the (western) eastern Uttarakhand and western Nepal. Also, the satellite observations and ERA5 diagnosed diabatic heating structure suggest that precipitating systems at higher (foothill)

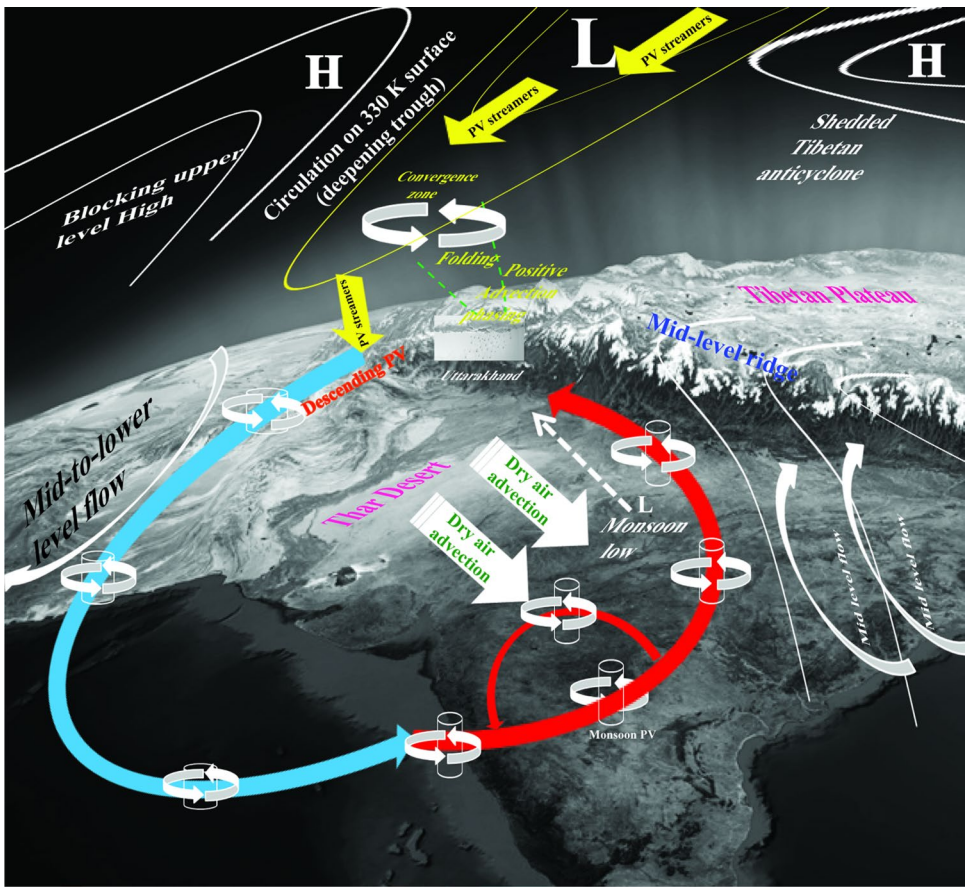

Fig. 17 A schematic of the processes described in this study

elevations of Uttarakhand contribute to upper (lower) tropospheric heat sources. In other words, larger sub-synoptic rain amounts came from shorter but copious spells with possibilities of convective regeneration/stationary convective cells at the same location along the lower elevations, while relatively less abundant hourly amounts but more incessant for longer periods from organized cloud clusters at higher elevations.

Acknowledgements The authors acknowledge The Director, Indian Institute of Tropical Meteorology (IITM), Pune, India, for the encouragement and support for this work. We thank the anonymous reviewers for providing valuable comments. This work is carried out under the Ministry of Earth Sciences (MoES), Government of India—Belmont Project Globally Observed Teleconnections and their role and representation in Hierarchies of Atmospheric Models (GOTHAM). The authors also acknowledge TRMM dataset archived and distributed by the Goddard Distributed Active Archive Center (https://pmm.nasa.gov), EUMETSAT for the METEOSAT-7 imagery datasets (https://eoportal.eumetsat.int) and the fifth-generation of ECMWF atmospheric reanalyzes (ERA5) products obtained from the Copernicus Climate Change Service Climate Data Store (CDS; https://cds.climate.copernicus.eu). Utilization of high performance computing facility at IITM for processing the datasets is acknowledged.

References

Anthes RA, Hoke JE (1975) The effect of horizontal divergence and the latitudinal variation of the Coriolis parameter on the drift of a model hurricane. Mon Weather Rev 103:757–763

Appenzeller C, Davies HC (1992) Structure of stratospheric intrusions into the troposphere. Nature 358:570–572

Bedka KM, Brunner JC et al (2010) Objective satellite-based overshooting top detection using infrared window channel brightness temperature gradients. J Appl Met Clim 49:181–202. https://doi.org/10.1175/2009JAMC2286.1

Bharti V, Singh C, Ettema J, Turkington TR (2016) Spatio-temporal characteristics of extreme rainfall events over the Northwest Himalaya using satellite data. Int J Climatol 36:3949–3962. https://doi.org/10.1002/joc.4605

Bluestein H (1992) Synoptic-dynamic meteorology in midlatitudes. Oxford Univ Press, Oxford, p 431

Boers N, Goswami A et al (2019) Complex networks reveal global pattern of extreme-rainfall teleconnections. Nature. https://doi.org/10.1038/s41586-018-0872-x

Chaudhuri C, Tripathi S, Srivastava R, Misra A (2015) Observation- and numerical analysis-based dynamics of the Uttarkashi cloudburst. Ann Geophys 33:671–686. https://doi.org/10.5194/angeo-33-671-2015

Chen P (1995) Isentropic cross-tropopause mass exchange in the extratropics. J Geophy Res 100:16661–16673

Chevuturi A, Dimri AP (2016) Investigation of Uttarakhand (India) disaster-2013 using weather research and forecasting model. Nat Hazards 82:1703–1726

Coumou D, Petoukhov V et al (2014) Quasi-resonant circulation regimes and hemispheric synchronization of extreme weather in boreal summer. Proc Natl Acad Sci 111:12331–12336

Danielsen EF (1968) Stratospheric-tropospheric exchange based on radioactivity, ozone and potential vorticity. J Atmos Sci 25:502–518

Dobhal DP, Gupta AK, Mehta M, Khandelwal DD (2013) Kedarnath disaster: facts and plausible causes. Curr Sci 105:171–174

Doswell CA (1987) The distinction between large-scale and mesoscale contribution to severe convection: a case study example. Weather Forecast 2:3–16

Dube A, Ashrit R et al (2014) Forecasting the heavy rainfall during Himalayan flooding—June 2013. Weather Clim Extremes 4:22–34. https://doi.org/10.1016/j.wace.2014.03.004

Dubey CS, Shukla DS et al (2013) Orographic control of the Kedarnath disaster. Curr Sci 105:1474–1476

Foresti L, Pozdnoukhov A (2012) Exploration of Alpine orographic precipitation patterns with radar image processing and clustering techniquies. Met Appl 19:407–419

Fujita TT (1958) Structure and movement of a dry front. Bull Am Meteorol Soc 39:574–582

Guhathakurta P, Sreejith OP, Menon PA (2011) Impact of climate change on extreme rainfall events and flood risk in India. J Earth Sys Sci 120:359–373

Hazra A, Chaudhari HS et al (2017) Role of interactions between cloud microphysics, dynamics and aerosol in the heavy rainfall event of June 2013 over Uttarakhand, India. Q J R Met Soc 143:986–998

Hersbach H, Dee D (2016) ERA5 reanalysis is in production, ECMWF Newsletter 147. ECMWF, Reading

Hoch J, Markowski P (2005) A climatology of springtime dryline position in the U.S., Great Plains region. J Clim 18:2132–2137

Holton J, Hakim GJ (2013) An introduction to dynamic meteorology. Academic Press, New York, p 552

Holton JR, Haynes PH et al (1995) Stratosphere-troposphere exchange. Rev Geophys 33:403–440

Homeyer CR, Bowman KP (2013) Rossby wave breaking and transport between tropics and extratropics above the subtropical jet. J Atmos Sci 70:607–626

Hoskins BJ, McIntyre ME, Robertson AW (1985) On the use and significance of isentropic potential vorticity maps. Q J R Met Soc 111:877–946

Houze RA, McMurdie LA et al (2017) Multiscale aspects of the storm producing the June 2013 flooding in Uttarakhand, India. Mon Weather Rev 145:4447–4466. https://doi.org/10.1175/MWR-D-17-0004.1

Hsu CJ, Plumb RA (2000) Nonaxisymmetric thermally driven circulations and upper tropospheric monsoon dynamics. J Atmos Sci 57:1255–1276

Huffman GJ, Adler RF et al (2007) The TRMM multisatellite precipitation analysis: quasi-global, multi-year, combined-sensor precipitation estimates at fine scale. J Hydrometeorol 8:38–55. https://doi.org/10.1175/JHM560.1

Joseph S, Sahai AK et al (2015) North Indian heavy rainfall event during June 2013: diagnostics and extended range prediction. Clim Dyn 44:2049–2065. https://doi.org/10.1007/s00382-014-2291.5

Joshi V, Kumar K (2006) Extreme rainfall events and associated natural hazards in Alaknanda Valley, Indian Himalayan Region. J Mt Sci 3:228–236

Kaur S, Purohit MK (2014) Rainfall statistics of India—2013. India Meteorological Department, Report No. ESSO/IMD/HS/R.F.REPORT/02(2014)/18, p 99

Knippertz P, Martin JE (2007) The role of dynamic and diabatic processes in the generation of cut-off lows over Northwest Africa. Meteorol Atmos Phys 96:3–19

Kotal SD, Roy SS, Roy Bhowmik SK (2014) Catastrophic heavy rainfall episode over Uttarakhand during 16–18 June 2013—observational aspects. Curr Sci 107:234–245

Krishbaum DJ, Adler B et al (2018) Moist orographic convection: physical mechanisms and links to surface-exchange processes. Atmosphere. https://doi.org/10.3390/atmos9030080

Krishnamurti TN, Kumar V et al (2017) March of buoyancy elements during extreme rainfall over India. Clim Dyn 48:1931–1951. https://doi.org/10.1007/s00382-016-3183-7

Krishnan R, Zhang C, Sugi M (2000) Dynamics of breaks in the Indian summer monsoon. J Atmos Sci 57:1354–1372

Kumar P, Shukla BP, Sharma S, Kisthawal CM, Pal PK (2016) A high-resolution simulation of catastrophic rainfall over Uttarakhand, India. Nat Hazards 80:1119–1134. https://doi.org/10.1007/s11069-015-2013-2

Kunz A, Konopka P et al (2011) Dynamical tropopause based on isentropic potential vorticity gradients. J Geophys Res 116:D01110. https://doi.org/10.1029/2010JD014343

Maddox RA, Chappel CF, Hoxit LR (1979) Synoptic and meso-α scale aspects of flash flood events. Bull Am Meteorol Soc 60:115–123

Manish S, Mishra SK, Shuchi T (2013) The impact of torrential rainfall in Kedarnath, Uttarakhand, India during June, 2013. Int Res J Environ Sci 2:34–37

Martius O, Schwierz C, Sprenger M (2008) Dynamical tropopause variability and potential vorticity streamers in the northern hemisphere—a climatological analysis. Adv Atmos Sci 25:367–380

Morgenstern O, Davies HC (1999) Disruption of an upper level PV streamer by orography and cloud-diabatic effects. Contrib Atmos Phys 72:173–186

Mujumdar M, Preethi B et al (2012) The Asian summer monsoon response to the La Nina event of 2010. Meteorol Appl 19:216–225. https://doi.org/10.1002/met.1301

Nandargi S, Gaur A (2013) Extreme rainfall events over the Uttarakhand State (1901–2013). Int J Sci Res. https://ww.ijsr.net/archive/v4i4/SUB152991.pdf

Nandargi S, Gaur A, Mulye SS (2016) Hydrological analysis of extreme rainfall events and severe rainstorms over Uttarakhand, India. Hydrol Sci J 61:2145–2163. https://doi.org/10.1080/02626667.2015.1085990

North GR, Erukhimova TL (2009) Atmospheric thermodynamics. Cambridge University Press, Cambridge, p 267

Orlanksi I (1975) A rational subdivision of scales for atmospheric processes. Bull Am Meteorol Soc 56:527–530

Pant GB, Kumar PP, Revadekar JV, Singh N (2018) Climate change in the Himalayas. Springer, Berlin, p 172

Parida BR, Behera SN et al (2017) Evaluation of satellite-derived rainfall estimates for an extreme rainfall event over Uttarakhand, Western Himalayas. Hydrology. https://doi.org/10.3390/hydrology4020022

Petrukhov V, Rahmstorf S, Petri S, Schellnhuber HJ (2013) Quasi-resonant amplification of planetary waves and recent Northern Hemisphere weather extremes. Proc Natl Acad Sci 110:5336–5341

Popovic JM, Plumb RA (2001) Eddy shedding from the upper-tropospheric Asian monsoon anticyclone. J Atmos Sci 58:93–104

Priya P, Krishnan R, Mujumdar M, Houze RA (2017) Changing monsoon and mid-latitude circulation interactions over the western Himalayas and possible links to occurrences of extreme precipitation. Clim Dyn 49:2351–2364. https://doi.org/10.1007/s00382-016-3458-z

Rajeevan M, Gadgil S, Bhate J (2010) Active and break spells of the Indian summer monsoon. J Earth Syst Sci 119:229–248

Rajesh PV, Pattanaik S et al (2016) Role of land state in a high-resolution mesoscale model for simulating the Uttarakhand heavy rainfall event over India. J Earth Sys Sci 125:475–498

Ranalkar MR, Chaudhari HS et al (2016) Incessant rainfall event of June 2013 in Uttarakhand, India: Observational perspectives. In: Ray K, et al. (eds) High-impact weather events over the SAARC region. Springer, Berlin, pp 303–312

Ranalkar MR, Chaudlhari H et al (2016) Dynamical features of incessant heavy rainfall event of June 2013 over Uttarakhand, India. Nat Hazards 80:1579–1601. https://doi.org/10.1007/s11069-015-2040-z

Rasmussen KL, Houze RA (2012) A flash flooding storm at the steep edge of high terrain: disaster in the Himalayas. Bull Am Meteorol Soc 93:1713–1724. https://doi.org/10.1175/BAMS-D-11-00236.1

Ray K, Bhan SC, Devi SS (2014) A meteorological analysis of very heavy rainfall event over Uttarakhand during 14–17 June 2013. Monsoon Report 2013, India Meteorological Department, Meteorological Monograph ESSO/IMD/SYNOPTIC MET/01-2014/15:37-54

Romero R, Doswell CA, Ramis C (2000) Mesoscale numerical study of two cases of long-lived quasi-stationary convective systems over Eastern Spain. Mon Weather Rev 128:3731–3751

Sawyer JS (1947) The structure of the intertropical front over northwest India during the southwest monsoon. Q J R Meteorol Soc 73:346–369. https://doi.org/10.1002/qj.49797331709

Schmetz J, Tjemkes SA et al (1997) Monitoring deep convection and convective overshooting with METEOSAT. Adv Sp Res 19:433–441

Shekhar MS, Pattanayak S et al (2015) A study of heavy rainfall event around Kedarnath area (Uttarakhand) on 16 June 2013. J Earth Syst Sci 124:1531–1544

Sikka DR, Ray K, Chakravarthy K, Bhan SC, Tyagi A (2015) Heavy rainfall in Kedarnath Valley during advancing monsoon phase in June 2013. Curr Sci 109:353–361

Soderholm B, Ronalds B, Kirshbaum J (2014) The evolution of convective storms initiated by an isolated mountain ridge. Mon Weather Rev 142:1430–1451

Srivastava AK, Guhathakurta P (2013) Climate diagnostics bulletin of India June 2013, near real-time analysis, issue 208, India Meteorological Department, Ministry of Earth Sciences, Earth System Science Organisation, Government of India, p 23

Vellore RK, Krishnan R et al (2014) On the anomalous precipitation enhancement over the Himalayan foothills during monsoon breaks. Clim Dyn 43:2009–2031. https://doi.org/10.1007/s00382-013-2024-1

Vellore RK, Kaplan ML et al (2016) Monsoon-extratropical circulation interactions in Himalayan extreme rainfall. Clim Dyn 46:3517–3546. https://doi.org/10.1007/s00382-015-2784-x

Wernli H, Sprenger M (2007) Identification of ERA-15 climatology of potential vorticity streamers and cutoffs near extratropical tropopause. J Atmos Sci 64:1569–1586

Xavier A, Manoj MG, Mohankumar K (2018) On the dynamics of an extreme rainfall event in northern India in 2013. J Earth Syst Sci. https://doi.org/10.1007/12040-018-0931-6

Yanai M, Esbensen S et al (1973) Determination of bulk properties of tropical cloud clusters from large-scale heat and moisture budgets. J Atmos Sci 30:611–627